

## 4.06 Dynamic Shear Rupture in Frictional Interfaces: Speeds, Directionality, and Modes

**A. J. Rosakis**, California Institute of Technology, Pasadena, CA, USA

**K. Xia**, University of Toronto, Toronto, ON, Canada

**G. Lykotrafitis**, Massachusetts Institute of Technology, Cambridge, MA, USA

**H. Kanamori**, Seismological Laboratory, Caltech, Pasadena, CA, USA

© 2007 Elsevier B.V. All rights reserved.

---

4.06.1	<b>Introduction</b>	153
4.06.2	<b>Experimental Techniques for Creating Earthquakes in the Laboratory</b>	154
4.06.2.1	Early Experimental Studies	154
4.06.2.2	Experimental Design Philosophy	156
4.06.2.2.1	Simulating tectonic loading	156
4.06.2.2.2	Simulating the nucleation process	157
4.06.2.2.3	Choosing appropriate model materials and diagnostics	158
4.06.3	<b>Supershear and Sub-Rayleigh to Supershear Transition in Homogeneous Fault Systems</b>	160
4.06.3.1	Purely Sub-Rayleigh and Purely Supershear Earthquake Ruptures	161
4.06.3.2	The Experimental Visualization of the Sub-Rayleigh to Supershear Earthquake Rupture Transition	163
4.06.3.3	A Theoretical Model for the Sub-Rayleigh to Supershear Transition	164
4.06.3.4	Discussion	167
4.06.4	<b>Directionality of Ruptures along Faults Separating Weakly Dissimilar Materials: Supershear and Generalized Rayleigh Wave Speed Ruptures</b>	167
4.06.4.1	Two Types of Ruptures along Inhomogeneous Fault Systems	168
4.06.4.2	Experimental Setup	170
4.06.4.3	Experimental Results	171
4.06.4.4	Comparison of the Experimental Results to Early Numerical and Theoretical Studies	173
4.06.4.5	The Parkfield Earthquake Discussion in the Context of Experiments and of Recent Numerical Studies	174
4.06.4.6	Discussion of the Historic, North Anatolian Fault Earthquake Sequence in View of the Experimental Results	175
4.06.5	<b>Observing Crack-Like, Pulse-Like, Wrinkle-Like and Mixed Rupture Modes in the Laboratory</b>	177
4.06.5.1	Experimental Investigation of Dynamic Rupture Modes	179
4.06.5.1.1	Specimen configuration and loading	180
4.06.5.1.2	Using particle velocimetry to measure slip and opening histories	181
4.06.5.2	Visualizing Pulse-Like and Crack-Like Ruptures in the Laboratory	181
4.06.5.3	Wrinkle-Like Opening Pulses along Interfaces in Homogeneous Systems	185
4.06.5.4	Discussion	187
	<b>References</b>	189

---

### 4.06.1 Introduction

The dramatic progress of research on earthquake rupture in the last decades along with advances in the various branches of geophysics has decisively

improved our understanding of seismic source events. A tremendous scientific activity including theoretical seismomechanics studies, field data processing, and laboratory investigations have answered many outstanding questions on earthquake dynamics.

Other problems yet remain to be solved whereas new questions have recently emerged. One of these questions is related to the ability of laboratory experiments to faithfully ‘mimic’ natural earthquake rupture events. In particular, this question is concerned with the ‘scalability’ of the laboratory results and observations. Can conclusions regarding the nature of dynamic rupture (e.g., modes, speeds, directionality etc.), obtained from such experiments, be accurately transferred from the laboratory scale (meters) to the natural earthquake rupture scale (hundred of kilometers)? Another question relates to similar issues in modeling. Do mechanics models and numerical simulations of rupture also suffer from scaling issues and do they need to first be validated by direct comparison to experiments before their results are extrapolated to the scale of rupture processes in the Earth’s crust? These are some of the questions which, although only partially addressed here, have motivated much of the work reviewed in the present chapter.

In this chapter, we first review past work on experimental simulations of earthquake rupture in the laboratory. We describe the basic traditional experimental techniques used in the last few decades and we then focus on a new experimental design philosophy introduced by the authors. This new approach to laboratory earthquakes has resulted in an experimental configuration particularly suited to the study of fast rupture events.

Following the description of the design philosophy, the chapter also concentrates on experimental results which demonstrate the attainability of inter-sonic rupture speeds (i.e., speeds in the interval between the shear and the dilatational wave speeds) and elucidate the sub-Rayleigh to supershear transition phenomenon in homogeneous fault systems. This transition is discussed in the light of well-established theoretical and numerical models based on the principles of fracture mechanics. In addition, recent field evidence of inter-sonic rupture that has occurred during natural earthquakes is presented and compared to the experimental observations.

The issue of the directionality of ruptures along faults separating weakly dissimilar materials is currently in the center of a very active debate between seismologists. In the present chapter, theoretical analyses together with field evidence and recent experimental and numerical results are utilized to provide a complete picture of the state of contemporary knowledge on this problem.

Finally, the various rupture modes (crack-like, pulse-like, wrinkle-like) which have been proposed

on the basis of field evidence and theoretical analyses are critically discussed. Experimental results, which show that the activation of these modes in the laboratory scale is possible, are presented.

Here, we have made the conscious decision not to include an extensive general introduction to this article. Instead, we have chosen to strengthen the introductory comments of individual sections and to blend reference to previous and current work within each section.

## **4.06.2 Experimental Techniques for Creating Earthquakes in the Laboratory**

### **4.06.2.1 Early Experimental Studies**

The first efforts of simulating earthquakes in the laboratory have utilized the classic block-slider configuration. Based on valuable observations gathered through this configuration, [Brace and Byerlee \(1966\)](#) have proposed that stick-slip may be an important mechanism for shallow earthquakes occurring along pre-existing faults. The basic assumption of the block-slider model is that the sliding rock blocks are rigid so that edge effects, leading to an initially nonuniform stress distribution along the interface, can be ignored. Under the rigidity assumption, friction along the interface can be assumed uniform and as a result only the displacement history of the slider needs to be measured. This assumption is clearly a very strong one since the Earth’s crust is far from being rigid during earthquake faulting. Although the block-slider model experiments do provide useful insight into some aspects of earthquake mechanics, such models are more appropriate for providing frictional constitutive information instead of modeling the detailed mechanics of earthquake rupture. Indeed, based on the pioneering experimental results of [Dieterich \(1979\)](#), the famous state- and rate-dependent friction law was formulated by [Ruina \(1983\)](#) and [Rice \(1983\)](#).

There are two configurations suitable for producing laboratory earthquakes, namely those of direct shear and of biaxial compression ([Brune, 1973](#); [Johnson and Scholz, 1976](#); [Wu \*et al.\*, 1972](#)). In order to extract meaningful rupture dynamics information from these configurations, the assumption of rigidity should be abandoned. Indeed, if strain gauges are attached along the fault in a two-dimensional (2-D) domain, the dynamic strain history resulting from the rupture can be recorded at various points. With

this modification, rupture velocities can also be estimated (Brune, 1973; Johnson and Scholz, 1976; Wu *et al.*, 1972) in addition to the dynamic friction-slip relation (Dieterich and Kilgore, 1994; Ohnaka and Shen, 1999; Okubo and Dieterich, 1984). However, strain gauges have approximate sizes of few millimeters, and this limits the spatial resolution of these discrete measurements. As a result, the data are point-wise, averaged, and are arguably difficult to interpret. For example, although supershear ruptures were suggested by this type of experiment (Johnson and Scholz, 1976; Okubo and Dieterich, 1984; Wu *et al.*, 1972), this evidence was considered far from being conclusive due to the ‘averaged’ quality of the data. Furthermore, since the diagnostics system (the Wheatstone bridge and oscilloscope) was triggered by one of the strain gauge signals and there was no information on the exact time and location of the nucleating point of earthquake (hypocenter), the sampling rate was necessarily set too low to capture the whole process. This has limited the time resolution of the measurements. Despite their shortcomings, these early studies have produced very valuable information concerning the nature and modes of frictional sliding. Indeed, by using this type of setup, the two important phenomena of frictional healing and velocity weakening were first observed by Scholz *et al.* (1972) and by Dieterich (1972).

Recently, two important modifications of the original block-slider model were introduced. The first one involved introducing a granular layer into the sliding interface to simulate the fault core (Gu and Wong, 1994). The second one involved using soft materials (e.g., foam rubber) and multipoint measurements performed by burying accelerometers inside meter-sized blocks (Brune, 1973; Brune *et al.*, 1993). The first type of test usually ignored the dynamic features of the earthquake, and is thus beyond the scope of this chapter. As to the second type of test, namely, the ‘foam model’, the usage of slow wave speed material has some distinct advantages over using rocks in that: (1) the whole process can be captured without the need of high sampling rates or high-speed photography and (2) 3-D effects can be more effectively addressed, since it is relatively easy to bury gauges inside the model. However, some concerns exist regarding the model material itself. These include its nonlinear and viscous nature and the special frictional properties of the foam rubber (the coefficient of friction can be larger than unity). Regarding their constitutive behavior, foam rubbers can sustain large deformations and are not well

described by the theory of linear elasticity. The presence of material nonlinearities (both kinematic and constitutive) raises concerns regarding the scalability of the results from the laboratory scale to naturally occurring earthquake ruptures. This together with their known viscoelastic response makes foam models unlikely candidates to simulate earthquakes, which occur in much stiffer and more brittle materials (i.e., rocks) and also involve sliding processes extending over lengths that are four to five orders of magnitude longer than in the laboratory. Furthermore, like all other direct shear-type experiments, the ‘foam model’ has also suffered from unavoidable edge effects as first pointed out by Scholz *et al.* (1972). Despite the few shortcomings described above, it should be emphasized that the foam rubber model has produced very interesting observations whose scientific value has been to elucidate some of the basic physics governing the sliding of frictional interfaces (Anooshehpour and Brune, 1994, 1999; Brune and Anooshehpour, 1997; Brune *et al.*, 1993).

At least three important simultaneously acting prerequisites are needed in order for an earthquake to occur either in the laboratory or in the Earth’s crust. These are: proper tectonic loading, a pre-existing fault, and the occurrence of a certain type of triggering mechanism. The first two prerequisites were very well simulated and controlled in the previously mentioned block slider and foam rubber models. However, the triggering of the rupture was mainly left uncontrolled and was dominated by the configuration edge effects discussed above. The triggering mechanism is important for both the earthquake process and its subsequent evolution (Lu *et al.*, 2005). In experiments, control of the triggering mechanism is crucial since it effects the synchronization of high-speed diagnostics and also serves as an important boundary/initial conditions that may affect the repeatability and the interpretation of the results. Except for one particular study specifically targeting the problem of the dynamic triggering of earthquakes by incoming Rayleigh waves (Uenishi *et al.*, 1999), this aspect has largely been ignored by the previous literature. In this important investigation, two photoelastic polymer plates of different sizes were held together at their convex sides to form a fault (line of frictional contact) with an extended free surface. A Rayleigh wave pulse was subsequently generated on the free surface by a point explosion and this wave propagated along the free surface toward the contact part (simulated fault). The incoming Rayleigh pulse was used to trigger dynamic slip along the fault in a controlled and repeatable fashion. In addition to

controlling rupture initiation, these experiments were also the first ones to feature the use of full-field optical diagnostics to study the dynamic rupture process in ‘incoherent’ (frictional) interfaces.

In addition to the experimental studies described above, there also exists a class of dynamic shear fracture experiments originating from the engineering community which are closely related to the phenomenon of geological fault rupture. As reviewed by Rosakis (2002), fracture mechanics are recently paying more and more attention to the dynamic shear rupture propagating along material interfaces which are becoming common in modern engineering structures and composite materials. These interfaces usually feature finite strength and toughness and can resist both opening and shear loading. They are often referred to as ‘coherent’ interfaces. Since they are in general weaker than the constituent matrix material, these interfaces often trap dynamic ruptures, of both the opening and shear types and serve as sites of catastrophic failure. On a much larger length scale, crustal faults provide natural weak frictional interfaces where shear-dominated earthquake ruptures occur under the superimposed action of tectonic pressure. Experimental methods for dynamic fracture mechanics, such as photoelasticity and coherent gradient sensing (CGS) combined with high-speed photography, have been applied successfully in the experimental study of shear ruptures propagating dynamically along coherent interfaces in engineering composites of various types (Coker and Rosakis, 2001; Coker *et al.*, 2003; Lambros and Rosakis, 1995; Rosakis *et al.*, 1998, 1999; 2000). These two diagnostic techniques, which are 2-D in nature, are able to provide very valuable full-field and real-time stress information. Specifically, the photoelastic method, which measures maximum in-plane shear stress contours, is an attractive candidate for the study of shear-dominated processes such as earthquake ruptures.

Further discussion of experimental methodologies and results pertaining to the investigation of various modes of rupture can be found in Section 4.06.5.1. In the following section, we present the principles that have guided the design of simple experiments involving incoherent (frictional) interfaces whose purpose has been to simulate earthquake rupture in a highly controlled laboratory setting.

#### 4.06.2.2 Experimental Design Philosophy

One goal in designing dynamic frictional experiments simulating earthquake rupture has been to create a

testing environment or platform which could reproduce some of the basic physics governing the rupture dynamics of crustal earthquakes while preserving enough simplicity so that clear conclusions can be obtained by pure observation. Another goal has been to ensure that this platform would be versatile enough to accommodate increasing levels of modeling complexity. We have concentrated in creating experiments that are well instrumented and feature diagnostics of high temporal and spatial resolution. In order to keep the design as simple as possible, we have decided to first concentrate on experiments involving essentially 2-D processes which may be thought of as ‘experimental’ equivalents of the multiplicity of 2-D numerical models of rupture which exist in the open literature. Because of its predominant two dimensionality this configuration is perhaps better suited to mimic processes corresponding to larger earthquake events which have already saturated the seismogenic zone and as such, involve primarily 2-D, mode-II rupture growth. The design of the generic experimental configuration, the earthquake triggering mechanism, and the choice of model materials and diagnostics are guided by the following principles:

##### 4.06.2.2.1 Simulating tectonic loading

As shown in Figure 1, the crust is simulated by a ‘large’ photoelastic plate with a thickness of 9.5 mm and 150 mm × 150 mm in 2-D plane dimensions. The plate is large enough so that during the time window of observation there are no reflected wave arrivals. The plate is cut into two identical quadrilaterals, which are then put together, and the frictional interface is used to simulate a fault. The angle of the fault line to the horizontal is denoted by  $\alpha$  while the uniaxial pressure acting at the top and the bottom ends of the sample is denoted by  $P$ . Both  $P$  and  $\alpha$  are system variables. Following these definitions, the resolved shear traction  $\tau$  and the resolved normal traction  $\sigma$  along the fault can be expressed in terms of angle  $\alpha$  and pressure  $P$  as

$$\tau = P \sin \alpha \cos \alpha \quad \text{and} \quad \sigma = P \cos^2 \alpha \quad [1]$$

To make the connection with commonly used geophysics terminology, a dimensionless factor  $s$ , which is often used by seismologists to describe the loading along faults with respect to the strength of the fault (Scholz, 2002), is introduced. By invoking the slip-weakening frictional model (Palmer and Rice, 1973) which is shown schematically in Figure 1(c), and by denoting the maximum strength of the fault by  $\tau^j$  and

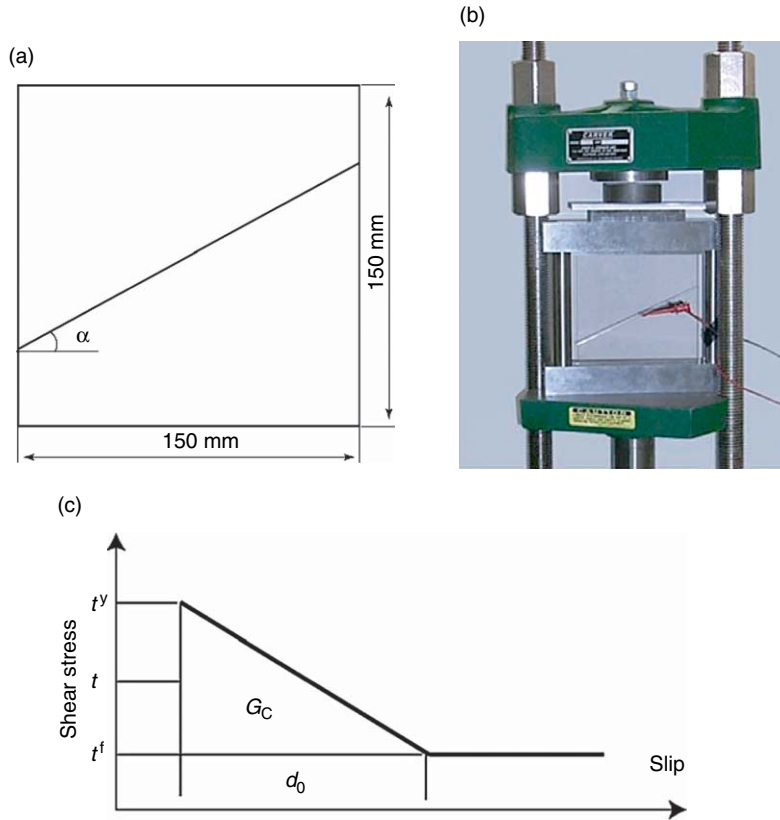


**Figure 1** Laboratory fault model (a) and the loading fixture inside a hydraulic press (b). Slip-weakening frictional law (c).

the final strength of the fault by  $\tau^f$ , this loading factor (or dimensionless driving force)  $s$  is defined by  $s = (\tau^y - \tau) / (\tau - \tau^f)$ . According to the linear slip-weakening fault strength model,  $\tau^y$  is the static frictional strength while  $\tau^f$  is the dynamic frictional strength of the interface. By denoting the static and dynamic coefficients of frictions by  $\mu^s$  and  $\mu^d$ , respectively, and by using eqn [1], the loading factor  $s$  corresponding to the geometry of the experiment of **Figure 1** becomes

$$s = (\mu^s \cos \alpha - \sin \alpha) / (\sin \alpha - \mu^d \cos \alpha) \quad [2]$$

As is obvious from eqn [2],  $s$ , and through it the earthquake rupturing process, can be controlled by varying the fault angle  $\alpha$  for given frictional properties of the fault in the experiments. The magnitude of the uniaxial pressure  $P$  does not appear in  $s$ . However, it controls the total amount of deformation and the total slip.

#### 4.06.2.2.2 Simulating the nucleation process

Researchers have tried to understand the nucleation process of earthquakes (triggering earthquake rupture) and indeed, they have shown that nucleation

can be understood by invoking proper friction relations (Dieterich, 1992; Lapusta and Rice, 2003; Uenishi and Rice, 2003). Unfortunately, it is impractical to explore the detailed physics of the nucleation event experimentally and instead, we have decided to mimic the way that triggering of rupture is achieved in numerical simulations. The triggering of natural earthquakes can be achieved either by an increase of the shear loading or by a decrease of the fault strength at a specific location. In the first case triggering due to a loading increase can occur dynamically if the requisite jump of shear stress is provided by stress waves generated by a nearby earthquake source. It can also occur quasi-statically due to the presence of inhomogeneities or stress concentrations along a fault (e.g., kinks or forks) which, as slip accumulates, may result in a critical increment of the local resolved shear stress on the interface. In the second case, triggering occurs through a local decrease of fault strength which may result, among other things, from the flow of pore fluid into the fault interstice generating a local release of fault pressure. Both mechanisms (pre-stress

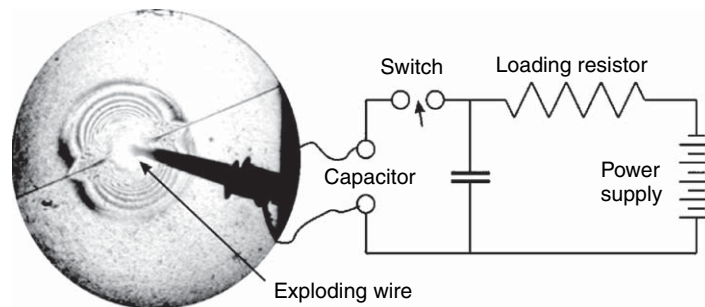


**Figure 2** Schematic drawing of the exploding wire system coupled with a photoelastic fault model. Isochromatic fringes due to the explosion are visible.

and pressure release) have been applied in numerical simulations of earthquake rupture dynamics (Aagaard *et al.*, 2001; Andrews, 1976; Andrews and Ben-Zion, 1997; Cochard and Rice, 2000; Fukuyama and Madariaga, 1998).

In the laboratory earthquake models described in this chapter, the triggering mechanism is a local pressure release, which is achieved by the exploding wire technique shown in **Figure 2**. A capacitor is charged by a high-voltage power supply. The charging time is determined by the resistance of the charging resistor and the capacity of the capacitor. Upon closing the switch, the electric energy stored in the capacitor causes a high current in a thin metal wire (buried inside a hole of 0.1 mm in diameter in the interface) for a short duration. The high current turns the metal wire into high-pressure, high-temperature plasma in approximately 10  $\mu\text{s}$ . The expansion of the high-temperature, high-pressure plasma causes a local pressure release. The adjustable power supply can provide electric potential in a wide range and different intensities and time durations of explosion can be obtained easily.

Before the explosion, the shear traction along the fault is less than the maximum static frictional strength. At the simulated hypocenter, after the explosion, the local normal traction on the fault is reduced and so is the static frictional strength. As a result, the applied shear traction, which is initially smaller than the static frictional strength and unaffected by the isotropic explosion, can be momentarily larger than the reduced frictional strength. The resulting net driving force, defined by the difference between the shear traction and the frictional resistance, drives the slip along the interface. Furthermore, the slip or the slip velocity also reduces the coefficient of friction as described by either a slip-weakening, or a velocity-weakening friction law. In other words, the frictional strength changes from

static to dynamic. If the original shear traction is larger than the dynamic friction, the slip continues to propagate away from the explosion site (corresponding to the hypocenter of an earthquake) where normal traction reduction due to the explosion is not important any more. In this way a spontaneous rupture or a laboratory earthquake is triggered.

#### 4.06.2.2.3 **Choosing appropriate model materials and diagnostics**

The diagnostic method of choice is dynamic photoelasticity. This technique is a classical method which measures the maximum shear stress in transparent, birefringent plates (Dally and Riley, 1991). As such the technique is very well suited for the study of shear-dominated processes. Two photoelastic solids, namely Homalite-100 and Polycarbonate, are used in all of the experiments described in the various sections of this chapter. The two materials have been chosen because of their enhanced birefringence relative to other transparent polymers such as polymethyl methacrylate (PMMA). Relevant properties of several photoelastic materials are listed in **Table 1**.

**Table 1** Summary of optical and mechanical properties of Homalite-100 and Polycarbonate

Material property	Homalite 100	Polycarbonate
Young's Modulus $E$ (MPa)	3860	2480
Poisson's Ratio $\nu$	0.35	0.38
Stress fringe value $f_\sigma$ ( $\text{kN m}^{-1}$ )	23.6	7.0
Yielding Stress $\sigma_Y$ (MPa)	48.3	34.5
P Wave Speed $C_P$ ( $\text{km s}^{-1}$ )	2.498	2.182
S Wave Speed $C_S$ ( $\text{km s}^{-1}$ )	1.200	0.960
Density $\rho$ ( $\text{kg m}^{-3}$ )	1230	1129

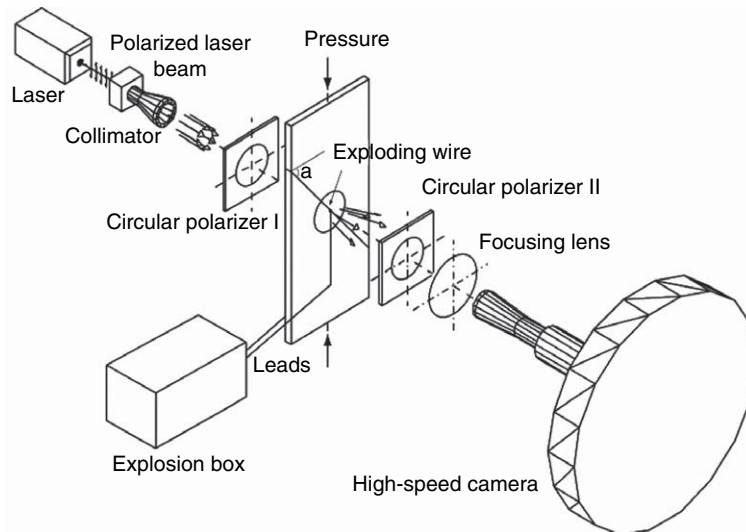


**Figure 3** The setup of dynamic photoelasticity combined with high-speed photography for laboratory earthquake studies.

The stress fringe values quoted in the table are for green light at a wave length 525 nm. The static elastic properties listed in **Table 1** are from the literature (Dally and Riley, 1991), while the dynamic elastic properties (wave speeds) were measured using 5 MHz ultrasonic transducers.

A typical of dynamic photoelasticity setup is shown in **Figure 3**. A polarized laser provides a high-intensity beam continuously at a power level of a few watts. The beam is then expanded by a collimator to a size of 100 mm or 130 mm in diameter. The large beam is transmitted through a combination of circular polarizers and the transparent photoelastic specimen, and it is arranged so that an isochromatic fringe pattern is obtained and focused into the camera. The isochromatic fringe pattern obtained from the two-dimensional photoelastic model gives fringes along which the in-plane principal stress difference  $\sigma_1 - \sigma_2$  is equal to a constant. When the fringe order  $N$  is known, the in-plane principal stress difference can be computed as follows:

$$\sigma_1 - \sigma_2 = Nf_\sigma / b \quad [3]$$

where  $b$  is the plate thickness of the model material. The high-speed camera (Cordin 220) used can take pictures at speeds up to  $10^8$  frames/second. In most experiments an interframe time of 2–4  $\mu\text{s}$  was used.

Another and perhaps the most important reason of using brittle polymers in our experiments is the small rupture nucleation length,  $L_G$ , resulting when such materials are frictionally held together by loads on the order of 10–20 MPa. As one can see by using eqn

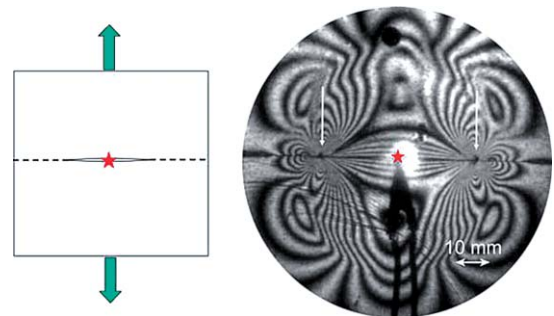


**Figure 4** Specimen configuration and photoelastic fringe pattern for self-similar crack growth of a mode-I (opening) crack along a coherent interface. White arrows indicate crack tips.

[1] in Section 4.06.3.3, these lengths are on the order of 5 mm and unlike rocks allow for relatively small laboratory specimen sizes. If rock samples were to be used instead of stiff polymers, the resulting rupture nucleation lengths would be approximately 30 times larger under similar far-field loading and surface finish. Finally, both Homalite and Polycarbonate are very brittle and are known to deform elastically at strain rates exceeding  $10^2 \text{ s}^{-1}$ .

An example of a dynamic photoelastic pattern corresponding to a ‘coherent’ (glued) and horizontal ( $\alpha = 0$ ) interface subjected to far-field tension is shown in **Figure 4**. This configuration which is of relevance to dynamic self-similar fracture of the mode-I (opening) type has been discussed in the recent work by Xia *et al.* (2006).

### 4.06.3 Supershear and Sub-Rayleigh to Supershear Transition in Homogeneous Fault Systems

The question of whether natural earthquake ruptures can ever propagate at supershear speeds was until recently a subject of active debate within the seismological community. This is because of the often insufficient field data, as well as the limited resolution and nonuniqueness of the inversion process. However, a recent experimental study (Xia *et al.*, 2004) has almost settled this question by demonstrating that under controlled laboratory conditions supershear frictional rupture can occur under conditions similar to those present in some natural settings. A widespread view in seismology speaks of crustal earthquake ruptures mainly propagating at sub-Rayleigh speeds between 0.75 and 0.95  $C_R$  (Kanamori, 1994). However, the multiplicity of independently collected evidence warrants further investigations of the mechanics of supershear rupture (velocity faster than the shear wave speed of the rock,  $C_S$ ) propagation. Whether and how supershear rupture occurs during earthquakes has an important implication for seismic hazard because the rupture velocity has a profound influence on the character of near-field ground motions (Aagaard and Heaton, 2004).

In the 8 August 2003 issue of *Science*, Bouchon and Vallee (2003) took advantage of the unusual length of the rupture event and used both seismic waves and geologically observed total slip distribution to infer the rupture velocity history of the great Ms 8.1 (Mw 7.8) central Kunlunshan earthquake that occurred in Tibet on 14 November 2001. This is an extraordinary event from the point of view of both earthquake dynamics and dynamic rupture mechanics. The rupture occurred over a very long, near-vertical, strike-slip fault segment of the active Kunlunshan fault and featured an exceptionally long (400 km) surface rupture zone and large surface slip (Lin *et al.*, 2002). Although it may not be unique, their modeling suggests speeds that are close to the Rayleigh wave speed of the crust,  $C_R$ , for the first 100 km of rupture growth, and transitioning to a supershear speed for the remaining 300 km of propagation. Their results were later corroborated by Das (private communication, 2006).

Recently, several other seismological reports also point to the possibility of supershear ruptures. These reports concentrate on events such as the 1979

Imperial Valley earthquake (Archuleta, 1984; Spudich and Cranswick, 1984), the 1992 Landers earthquake (Olsen *et al.*, 1997), and most recently the 2002 Denali earthquake in Alaska (Ellsworth *et al.*, 2004). The 1999 Izmit earthquake in Turkey (Bouchon *et al.*, 2001) is yet another event featuring a very long segment of supershear rupture growth. It should be noted here that for most of those examples mentioned above (Izmit and Denali excluded), the supershear ruptures occurred only on short patches along the whole rupture length and the results are not conclusive. Bouchon and Vallee's (2003) paper together with Das's work on Kunlunshan, as well as the work of Ellsworth *et al.* (2004) on Denali are the most recent of a series of investigations reporting supershear rupture growth occurring during 'large' earthquake events. Moreover, they present the first seismological evidence for transition from sub-Rayleigh to supershear.

Classical dynamic fracture theories of growing shear cracks have many similarities to the earthquake rupture processes (Broberg, 1999; Freund, 1990; Rosakis, 2002). Such theories treat the rupture front as a distinct point (sharp tip crack) of stress singularity. These conditions are close to reality in cases that feature strong 'coherent' interfaces of finite intrinsic strength and toughness. The singular approach ultimately predicts that dynamic shear fracture is allowed to propagate either at a sub-Rayleigh wave speed or at only one supershear speed, which is  $\sqrt{2}$  times the shear wave speed. As a result, it excludes the possibility of a smooth transition of a steady-state rupture from sub-Rayleigh to supershear speed for a steady-state rupture. The introduction of a distributed rupture process zone has allowed fracture mechanics to better approximate the conditions that exist during real earthquake events (Ida, 1972; Palmer and Rice, 1973). Based on this so-called cohesive zone fracture mode, there is a forbidden speed range between  $C_R$  and  $C_S$  (Burridge *et al.*, 1979; Samudrala *et al.*, 2002a, 2002b). In the sub-Rayleigh speed range all speeds are admissible, but only the Rayleigh wave speed is a stable speed; in the supershear speed range all speeds are admissible, but only speeds larger than  $\sqrt{2}C_S$  are stable (Samudrala *et al.*, 2002b). Ruptures with unstable speeds will accelerate to a stable speed as determined by the fault strength and the loading conditions. The theoretical results of the cohesive zone rupture model ultimately predict that earthquake ruptures can propagate either at Rayleigh wave speed or at supershear speeds lying within the interval between  $\sqrt{2}C_S$  and  $C_p$ .

Early theoretical results by Burridge and co-workers (Burridge, 1973; Burridge *et al.*, 1979), along with numerical results by Andrews (1976) and Das and Aki (1977) have predicted the possibility of supershear rupture and have alluded to a mechanism (Rosakis, 2002) for transition from the sub-Rayleigh to the supershear rupture velocity regime. This is often referred to as the ‘Burridge–Andrews’ mechanism. According to the 2-D Burridge–Andrews mechanism, a shear rupture accelerates to a speed very close to  $C_R$  soon after its initiation. A peak in shear stress is found sitting at the shear wave front and is observed to increase its magnitude as the main rupture velocity approaches  $C_R$ . At that point, the shear stress peak may become strong enough to promote the nucleation of a secondary microrupture whose leading edge propagates at a supershear speed. Shortly thereafter, the two ruptures join up and the combination propagates at a speed close to  $C_P$ , the longitudinal wave speed of the solids. It is interesting that this transition was also clearly visualized by recent 2-D, atomistic calculations (Abraham and Gao, 2000; Gao *et al.*, 2001) of shear rupture in the microscale, which provided an impressive demonstration of the length scale persistence (14 orders of magnitude difference between the nanoscale and the scale of natural earthquake rupture) of this sub-Rayleigh to supershear rupture transition mechanism. The Burridge–Andrews mechanism is also known as the mother–daughter mechanism in mechanics literature.

For mixed-mode (tensile and shear) ruptures, a different transition model has also been suggested (Geubelle and Kubair, 2001; Kubair *et al.*, 2002, 2003). Based on numerical simulation, they suggest that a mix-mode rupture can speed up and cross the forbidden speed range between  $C_R$  and  $C_S$  continuously. Finally, recent numerical investigations of frictional rupture have identified alternate, asperity based, mechanisms that provide a 3-D rationalization of such a transition (Day, 1982; Dunham *et al.*, 2003; Madariaga and Olsen, 2000). In this case, 3-D effects play an important role in the transition. The rupture front focusing effect provides extra driving force to speed up the spontaneous rupture in the supershear range.

The experimental confirmation of the possibility of supershear (intersonic) fracture followed many years after the first theoretical predictions. Indeed, the long series of experiments summarized in a recent review by Rosakis (2002) demonstrate that intersonic crack growth in constitutively homogenous systems featuring

coherent interfaces (interfaces with inherent strength) is possible and may also occur in various combinations of bimaterial systems. However, in all of the various cases discussed by Rosakis (2002), the cracks were nucleated directly into the intersonic regime and there was no observation of a transition from sub-Rayleigh to supershear speeds. This was due to the nature of the impact induced stress wave loading which was imparted in the absence of pre-existing static loading and the nature of the relatively strong coherence of the interface (provided by adhesive). The major differences between the conditions during earthquake rupture and those early fracture experiments have left questions regarding the plausibility of spontaneously generated intersonic rupture in frictionally held, incoherent interfaces unanswered. The recent work by Xia *et al.* (2004) on frictionally held interfaces has addressed this issue in detail. In the following sections, we will summarize their most important findings and we will attempt to relate these findings to field measurements related to recent natural earthquake events.

#### 4.06.3.1 Purely Sub-Rayleigh and Purely Supershear Earthquake Ruptures

In this section, experimental parameter ranges leading to either exclusively sub-Rayleigh or exclusively supershear ruptures will be discussed. The configuration of interest is the one described in Section 4.06.2.2. The physics governing possible transitions between these two speed regimes within a single rupture event will be examined later. Figure 5 shows two different experiments featuring sub-Rayleigh speed ruptures. In all the photographs, we can clearly see the circular shear wave front emitted from the simulated hypocenter. Rupture tips, characterized by the stress concentration (fringe concentrations in the photographs), are identified just behind the shear wave front. The P-wave is long gone out of the field of view (100 mm). The ruptures as shown in the photograph feature right lateral slip while the rupture tips are equidistant from the hypocenter (symmetric bilateral slip). From the rupture length history, it is possible to estimate the rupture velocity. In these two cases, the rupture velocities are very close to the Rayleigh wave speed of the material.

All experiments featuring lower inclination angles  $\alpha$  and lower magnitude of uniaxial compression pressure  $P$  involve exactly the same features and rupture speeds. This observation is consistent with many observations of earthquake rupture velocities in the

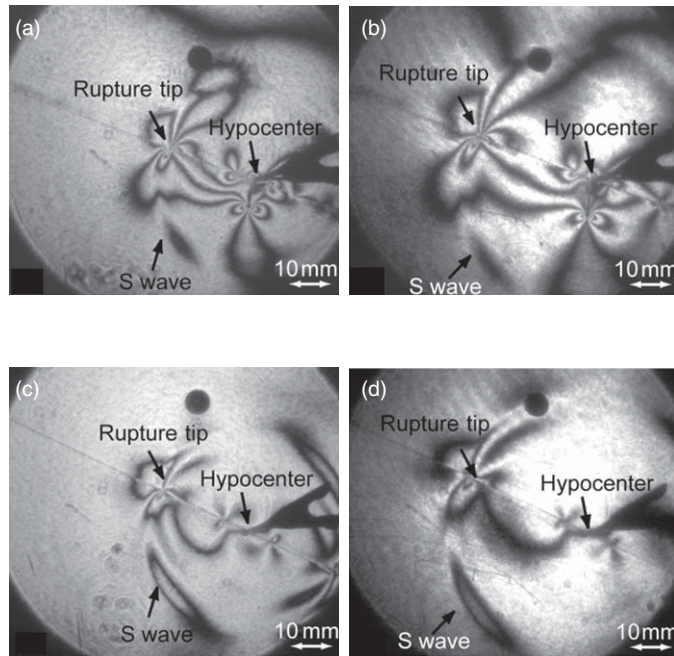


**Figure 5** Experimental results of purely sub-Rayleigh cases. (a) and (b) are from one experiment with a pressure of  $P = 13$  MPa and angle  $\alpha = 20^\circ$  at time instants of 28 and 38  $\mu\text{s}$ , respectively. (c) and (d) are from an experiment with a pressure of  $P = 7$  MPa and angle  $\alpha = 25^\circ$  at the time instants of 28 and 38  $\mu\text{s}$ , respectively. For (a) and (b), we can also identify two mode-I cracks in the lower half of the sample caused by the explosion itself. We expect that the effect of these cracks is localized.

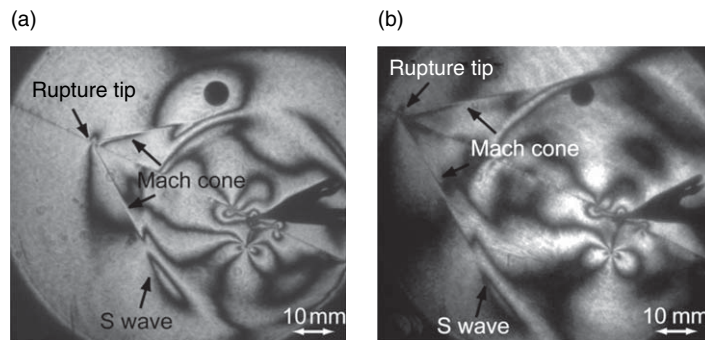


**Figure 6** Experimental results for the purely supershear case. (a) and (b) both correspond to an experiment with the pressure of  $P = 15$  MPa and angle  $\alpha = 25^\circ$  at the two time instants of 28 and 38  $\mu\text{s}$ , respectively.

field. As we have discussed earlier, in the sub-Rayleigh speed range the only stable rupture velocity is the Rayleigh wave speed according to various cohesive zone models of rupture. The experiments of Xia *et al.* (2004) described in this section confirm this observation.

In **Figure 6**, the inclination angle was kept at  $25^\circ$  while the pressure was increased to 15 MPa. For comparison purposes, the same time instants (28 and 38  $\mu\text{s}$  after nucleation) are displayed.

In this case, the circular traces of the shear wave are also visible and are at the same corresponding locations as in **Figure 6**. However, in front of this circle supershear disturbances (propagating to the left, marked in the photograph as the rupture tip and featuring a clearly visible Mach cone) are shown. The formation of the Mach cone is due to the fact that the rupture front (tip) is propagating faster than the shear wave speed of the material. For this case, the sequence of images, other than

those at 28 and 38  $\mu\text{s}$ , have a very similar form and reveal a disturbance that was nucleated as supershear. The speed history  $v(t)$  is determined independently by either differentiating the rupture length history record or measuring the inclination angle,  $\delta$ , of the shear shocks with respect to the fault plane, and using the relation  $v = C_S/\sin \delta$ . The speed was found to be almost constant and very close to the plane stress P-wave speed  $C_P$  of the material. These experiments provide the first evidence of supershear growth of a spontaneous shear rupture propagating along a frictional interface. The supershear rupture initiated right after the triggering of the earthquake rupture. This is determined from the fact that the Mach cones are nearly tangential to the shear wave front which was itself created at the time of rupture nucleation.

In previous experiments involving strong, coherent interfaces and impact induced stress wave loading, stable rupture velocities slightly exceeding  $\sqrt{2}C_S$  were observed (Rosakis *et al.*, 1999). This apparent discrepancy can be explained by referring to the rupture velocity dependence on the available energy per unit shear rupture advance within the supershear regime (Samudrala *et al.*, 2002b). This dependence was obtained by means of an analytical model of a dynamic steady state, shear rupture featuring a shear cohesive zone of the velocity weakening type. The initial, static, strength of the interface was represented by the parameter  $\tau_0$ . For a given normalized far-field loading level,  $\sigma_{12}^D/\tau_0$ , this energy, shown here in normalized form (Figure 7) as a function of rupture speed, attains a maximum value at speeds closer to  $\sqrt{2}C_S$  for interfaces that are ‘strong’. This is consistent with the purely singular

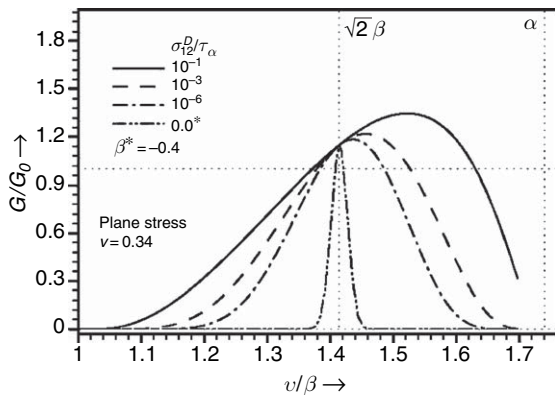


**Figure 7** Normalized energy release rate as a function of intersonic rupture speed. The figure illustrates that the energy flux available to the tip has a maximum at or above  $v = \sqrt{2}C_S$ .

prediction which corresponds to idealized interfaces of infinite strength. To this idealized case, ( $\tau_0 \rightarrow \infty$ ), the only value of rupture velocity corresponding to finite  $G$  is exactly  $\sqrt{2}C_S$ . For weaker interfaces (or higher driving stresses), this maximum moves toward  $C_P$ . In the situation described in this section, the interface is ‘weak’ and the driving force (resolved shear minus dynamic frictional force) is relatively large and constant. Hence, a rupture velocity close to  $C_P$  is expected.

#### 4.06.3.2 The Experimental Visualization of the Sub-Rayleigh to Supershear Earthquake Rupture Transition

As discussed earlier, investigating how supershear ruptures are nucleated experimentally is of great interest. For the experimental cases described in the above section, the supershear rupture event was nucleated immediately after triggering of the rupture event. Since the rupture velocity is controlled by both the inclination angle  $\alpha$  and the magnitude of uniaxial compression  $P$ , it is possible to vary both of them carefully to suppress or perhaps delay the appearance of supershear rupture. Specifically, the inclination angle  $\alpha$  was fixed at  $25^\circ$  while  $P$  was decreased in order to induce and capture the nucleation process of a supershear rupture.

Figures 8(a)–(c) corresponds to a case with an intermediate far-field pressure compared to the ones displayed in Figures 5(c) and 5(d) and Figure 6. Here, the angle is kept the same ( $25^\circ$ ) and the pressure is decreased to 9 MPa in an attempt to visualize a transition within our field of view (100 mm). Three different time instances of the same rupture event are displayed. In Figure 8(a), the circular traces of both P- and S-waves are visible, followed by a rupture propagating at  $C_R$ . In Figure 8(b), a small secondary rupture appears in front of the main rupture and propagates slightly ahead of the S-wave front. In Figure 8(c), the two ruptures coalesce and the leading edge of the resulting rupture grows at a speed of  $1970 \text{ m s}^{-1}$  which is very close to  $C_P$ . A well-defined ‘shear’ Mach cone is visible in Figure 8(c). Unlike Figure 6, the Mach lines are not tangential to the shear wave circle since the supershear rupture was not generated at initiation. Figure 8(d) displays the length versus time of the two ruptures, in which the length is directly read from the figure. The figure also compared the slopes to the characteristic wave speeds of the material before and after their coalescence. A magnified view

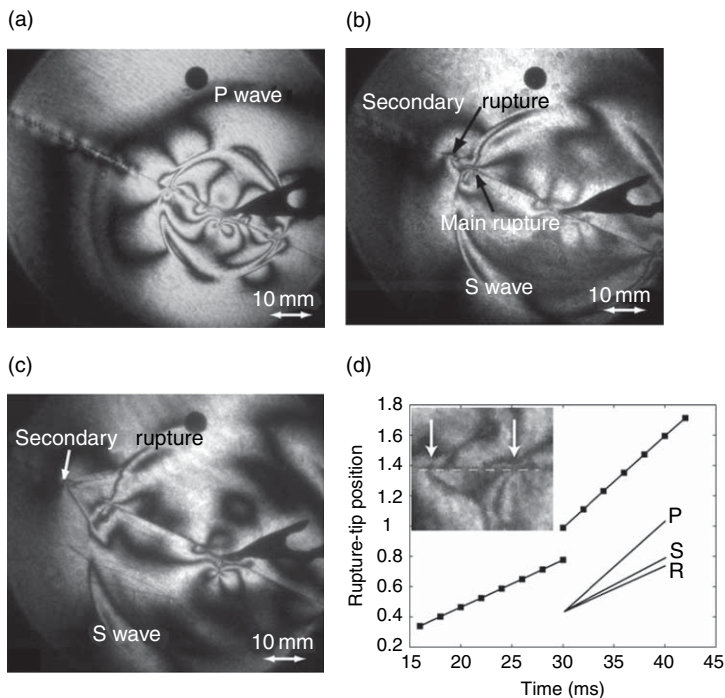


**Figure 8** Visualization of the sub-Rayleigh to supershear rupture transition.

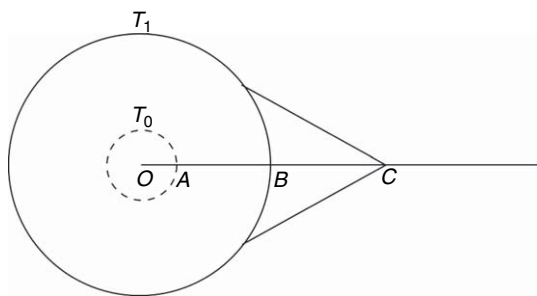


**Figure 9** Method of transition length  $L$  estimation.

of the secondary rupture as it nucleates in front of the main rupture is shown in the inset. Both ruptures are indicated by arrows. The transition length  $L$  for this case is approximately 20 mm, as is visually obvious by **Figure 8(b)**.

In cases where the transition length cannot be measured directly if it is too small, an indirect method is developed. As shown in **Figure 9**, at time  $T_0$ , the supershear rupture is nucleated at the intersection of the shear wave front and the fault line (point A). If the transition length  $L = OA$  is very small, spatial resolution may not be good enough to measure it accurately. Alternatively, a photograph may not have been taken at that instant. Assuming

that at all times before transition the rupture speed is very close to  $C_S$  and that the shear wave position (A) and supershear rupture-tip position (B) at a later time instance  $T_1$  can be measured, the transition length can be inferred by pure geometry. To do so we observe that relations  $OA = C_S T_0$ ,  $OB = C_S T_1$ , and  $AC = V(T_1 - T_0)$  hold provided that the supershear rupture tip also grows at a constant speed  $V > C_S$  (as confirmed by **Figure 8**).

A simple manipulation gives  $AC/OB = (1 - T_0/T_1)V/C_S$ , which leads to  $T_0 = [1 - (C_S/V)(AC/OB)]T_1$ . Multiplication of both sides of the last relation by  $C_S$  gives  $L = OA = C_S T_0 = [OB - OC \times C_S/V]$ . This relation allows for the estimation of the supershear rupture transition length,  $L$ , even if no photographic records have been obtained at or before the time instance of the transition. Several results listed in this chapter were either obtained or verified by using this method.

#### 4.06.3.3 A Theoretical Model for the Sub-Rayleigh to Supershear Transition

The above physical picture is comparable with the Burridge–Andrews mechanisms already described in the introduction of this chapter. **Andrews (1976,**

1985) quantified this transition in a parameter space spanned by a normalized supershear transition length  $L/L_C$  and the nondimensional driving stress parameter  $s$  [ $s = (\tau^y - \tau)/(\tau - \tau^f)$ ]. The parameters  $\tau$ ,  $\tau^y$ , and  $\tau^f$  are the resolved shear stress on the fault, the static frictional strength, and the dynamic strength of the fault, respectively; they describe the linear slip-weakening frictional law (Ida, 1972; Palmer and Rice, 1973) used in Andrews' computations.

The Andrews result can be symbolically written as  $L = L_C f(s)$ . The function  $f(s)$  has been given numerically by Andrews as an increasing function of  $s$ , and can be well approximated by the equation  $f(s) = 9.8(1.77 - s)^{-3}$ . The normalizing length  $L_C$  is the critical length for unstable rupture nucleation and is proportional to the rigidity  $G$  and to  $d_0$ , which is defined as the critical or breakdown slip of the slip-weakening model.  $L_C$  can then be expressed as

$$L_C = \frac{1 + v(\tau^y - \tau^f)}{\pi(\tau - \tau^f)^2} G d_0 \quad [4]$$

By adopting the above relation to the geometry of the experimental configuration and by using eqn [1], the transition length  $L$  is found to be inversely proportional to the applied uniaxial pressure  $P$  and to be governed by the following general functional form:

$$L = f(s) \frac{1 + v(\mu^s - \mu^d)}{\pi(\tan \alpha - \mu^d)^2} \frac{G d_0}{P} \quad [5]$$

Figure 10 displays the dependence of the transition length  $L$  on pressure from a set of experiments corresponding to the same inclination angle of  $25^\circ$

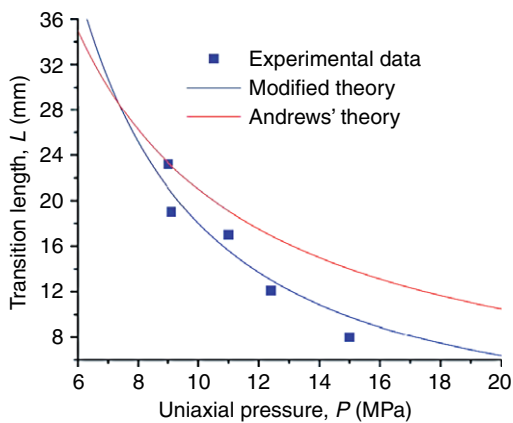


Figure 10 Transition length as a function of the far-field load.

( $s = 0.5$ ) and identical surface finish (roughness is about  $17 \mu\text{m}$ ). The static frictional coefficient was measured to be  $\mu^s = 0.6$  using the traditional inclined plane method. In this method, one block was placed on top of an inclined plane and the inclination angle until the block slides. By this way the critical inclination angle  $\Psi_C$  was measured. The static coefficient of friction was then determined from the relation  $\mu^s = \tan^{-1}(\Psi_C)$ . To estimate the average, steady state, dynamic frictional coefficient,  $\alpha$  was gradually increased from  $10^\circ$  to a critical angle  $\alpha_c$  at which slip was initiated under the action of far-field loads and the dynamic triggering. It was assumed that the shear traction was approximately equal to the dynamic frictional strength at this critical angle  $\alpha_c$ . This angle was found to be between  $10^\circ$  and  $15^\circ$ , from which the average coefficient of dynamic friction was estimated to be  $\mu^d = 0.2$ . This low value of dynamic friction coefficient is very consistent with recent experimental measurements conducted by Tullis and his research group at slip velocities approaching seismic slip rates (Di Toro *et al.*, 2004; Tullis and Goldsby, 2003). Using  $\mu^s = 0.6$  and  $\mu^d = 0.2$ , the experiments can be compared to the predictions of eqn [5] of Andrews' theory as shown in Figure 10. Although the theory qualitatively captures the decreasing trends of the experiments, the data exhibit a dependence on pressure that is visibly stronger than  $P^{-1}$ .

A natural way to modify Andrews' results and to introduce some scaling into the pressure dependence of  $L$  is to consider the effect of pressure on the critical breakdown slip  $d_0$ . As pointed out by Ohnaka, on the basis of frictional experiments on rocks, and as also supported by dimensional analysis, there exists a linear relation between a characteristic surface length (half-distance between contacting asperities, denoted as  $D$  in this case) and the critical slip distance  $d_0$  as (Ohnaka, 2003)

$$d_0 = c[(\tau^y - \tau^f)/\tau^f]^M D \quad [6]$$

where  $c$  and  $M$  are experimentally determined constants. In addition,  $D$  depends on the normal stress,  $\sigma$ , applied on the fault (which is  $\sigma = P \cos^2 \alpha$  in this case). As shown in Figure 11, a classical plastic contact model may be used to establish this dependence. In this model the average radius of  $n$  contacting asperities is  $a_0$  (assumed as a constant in this model). As the pressure over a macroscopic contact area  $A (=n\pi D^2)$  is increased, the number of contacts,

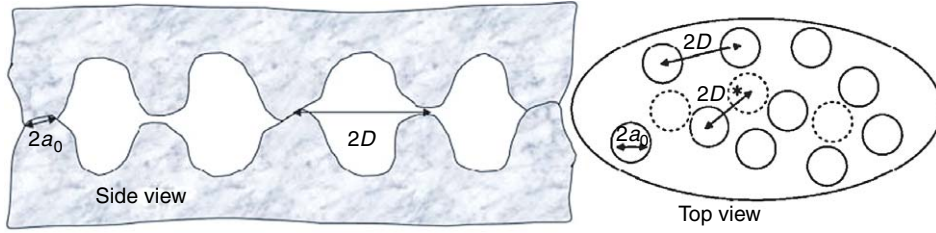


**Figure 11** Schematic drawing of the microcontact based frictional model. The top figure is the side view of the contact and the bottom figure is the top view. As the normal force increases, the number of contacts,  $n$ , increase.

$n$ , as well as the real contact area  $A_r (= n\pi a_0^2)$ , also increases.

By defining the hardness  $H$  as the ratio of the total normal force  $N$  to the real contact area  $A_r$  (Bowden and Tabor, 1986),  $N$  can be expressed as

$$N = HA_r = Hn\pi a_0^2 = \sigma A = AP \cos^2 \alpha \quad [7]$$

Substitution of  $A$  and  $A_r$  in terms of  $D$  and  $a_0$  gives  $D = \sqrt{H} a_0 \cos \alpha P^{-1/2}$ . Using the linear relation between  $D$  and  $d_0$ , the breakdown slip is further found to depend on the pressure as  $d_0 \sim P^{-1/2}$ . By substituting the above relations into the expression relating  $L$  and  $d_0/P$ , discussed above, a modified expression of transition length to pressure that features a stronger dependence ( $L \sim P^{-3/2}$ ) on pressure emerges. For the loading conditions and geometry of the experimental configuration presented in **Figure 1**, this expression becomes

$$L = f(s) \frac{1+v}{\pi} G \frac{\mu^s - \mu^d}{(\sin \alpha - \mu^d \cos \alpha)^2} 2c \left( \frac{\mu^s - \mu^d}{\mu^s} \right)^M \times \sqrt{H} a_0 P^{-3/2} \cos^{-1} \alpha \quad [8]$$

As shown in **Figure 10**, this modified relation agrees very well with the experimental data presented in this paper for appropriate choices of material and geometrical parameters of the micromechanics contact model. In plotting **Figure 10**, the hardness and the elastic constants of Homalite were used while the friction coefficients were taken to be  $\mu^s = 0.6$  and  $\mu^d = 0.2$  as estimated above. The values for the constants  $c$  and  $\mu$  were from the experiments of Ohnaka (2003). The asperity radius  $a_0$  was taken to be equal to  $1.78 \mu\text{m}$ , for a best fit to the experimental data. This value was found to be consistent to averaged measurements of asperity radii obtained through microscopic observations of the sliding surfaces. Relation [8] can also easily be generalized to biaxial loading conditions. Indeed, if  $P_1 = P$  and  $P_2 = bP$  denote the horizontal and vertical components of

the applied loads such a situation, the transition length can be expressed as

$$L = f[s(\alpha)] \frac{1+v}{\pi} G \frac{2c(\mu^s - \mu^d)^{1+M} (\cos^2 \alpha + b \sin^2 \alpha)^{1.5}}{[(1-b) \sin \alpha \cos \alpha - \mu^d (\cos^2 \alpha + b \sin^2 \alpha)]^2} \times (\mu^s)^{-M} \sqrt{H} a_0 P^{-1.5} \quad [9]$$

In addition to tectonic loading magnitude and direction relative to fault inclination, eqn [9] involves the material properties  $G$ ,  $v$ , and  $H$ , the frictional properties  $\mu^s$  and  $\mu^d$ , as well as fault related length scale  $a_0$ . Because of this, it can perhaps be used as a simple scaling relation connecting laboratory observations to reports of supershear transition in ‘large’ natural earthquake rupture events such as these related to 2001 Kunlunshan event in Tibet.

For making order of magnitude level contact with seismological applications, we rewrite the general form of eqn [5] in terms of the effective stress  $\tau^e = \tau - \tau^f$ , a commonly used and estimated seismological parameter. Equation [5] can be rewritten as

$$L = f(s) \frac{1+v}{\pi} (1+s) \frac{Gd_0}{\tau^e} \quad [10]$$

Application of this equation to both seismic faulting and laboratory data allows us to scale the transition length  $L$  from laboratory to seismological conditions. The effective stress  $\tau^e$  in our experiment is chosen to be of the same order of magnitude as that measured in seismology. The ratio of rigidity of the Earth’s crust to Homalite is about 25. From the experiment described in **Figure 8** ( $P = 9 \text{ MPa}$  and  $\alpha = 25^\circ$ ) the transition length is estimated to be  $L = 20 \text{ mm}$  from which  $d_0 = 10 \mu\text{m}$  is obtained using eqn [4]. The values of  $d_0$  for large earthquakes are often estimated as  $50 \text{ cm}$  to  $1 \text{ m}$  (Ide and Takeo, 1997). If  $s$  is approximately the same under laboratory and crustal conditions, the transition length for earthquakes can be estimated to be in the range between 25 and 50 km. Because  $s$  can be different and the estimate of  $d_0$  for earthquakes is very uncertain at present, this value

should only be taken as an order of magnitude estimate. Nevertheless, it is of the same order as that inferred for Kunlunshan (100 km) and for Denali (75 km). The large transition length required for supershear is perhaps one of the reasons that relatively few earthquake events have been observed to feature such high rupture velocities and that all of them correspond to large magnitude earthquakes. If the tectonic stress is well below the static fault strength (i.e., large  $\sigma$ ), the transition length becomes too large for many earthquake ruptures to attain supershear. The observation that during several large earthquakes the rupture velocity became very fast, possibly supershear, suggests that the tectonic stress is fairly close to the static fault strength (i.e., small  $\sigma$ ), which has important implications for the evolution of rupture in large earthquakes.

#### 4.06.3.4 Discussion

A final word of caution is in order here. It has recently been shown in recent preliminary numerical simulations of the homogeneous experiments described in this section (Lu *et al.*, 2005) that the detailed variation of the transition length on the load  $P$  may also strongly depend on the nature of the rupture nucleation process. The severity of this effect is still unknown. If this dependence proves to be significant, an experimental investigation involving various pressure release histories (intensities, rise times, and durations) will be necessary in order to complete the experimental investigation of supershear transition presented above. A related issue regarding the influence of nucleation conditions in a bimaterial setting (see Section 4.06.4) was recently discussed by Shi and Ben-Zion (2006).

#### 4.06.4 Directionality of Ruptures along Faults Separating Weakly Dissimilar Materials: Supershear and Generalized Rayleigh Wave Speed Ruptures

In most mature fault systems, the elastic properties vary across the fault plane (Magistrale and Sanders, 1995; Peltzer *et al.*, 1999) and also the shear wave speeds may vary by as much as 30% (Ben-Zion and Huang, 2002; Cochard and Rice, 2000). Recently, Rubin and Gillard (2000) studied several thousands of pairs of consecutive earthquakes that occurred on a segment of the central San Andreas fault, south of the

Loma Prieta rupture. Among the second events of each pair, they found that over 70% more occurred to the northwest than to the southwest. They interpret this asymmetry as being a result of the contrast in material properties across the fault. Indeed, at this location of the San Andreas Fault, the rock body is more compliant northeast of the fault than it is southwest (Eberhart-Phillips and Michael, 1998).

Early theoretical and numerical studies of rupture that employ various frictional laws with a constant coefficient of friction which would be independent of slip or slip rate (Adams, 1995; Andrews and Ben-Zion, 1997; Cochard and Rice, 2000; Harris and Day, 1997; Heaton, 1990; Ranjith and Rice, 1999; Rice *et al.*, 2001; Weertman, 1980) imply that if rupture occurs on the boundary between two frictionally held solids, having different elastic properties and wave speeds, such a rupture may preferentially propagate in a particular direction. This is the same direction as the direction of slip in the lower wave speed solid. This direction is often referred to as the ‘preferred’ direction (Ben-Zion 2001). Since such implied directionality of fault rupture may have a profound influence on the distribution of damage caused by earthquake ground motion, it would be extremely useful if this behavior could be confirmed under controlled laboratory conditions. While many of the physical aspects of dynamic rupture (including supershear) are recently becoming progressively clearer in relation to homogeneous faults (Ben-Zion, 2001; Rice, 2001; Rosakis, 2002; Xia *et al.*, 2004), the behavior of spontaneously nucleated ruptures in inhomogeneous faults, separating materials with different wave speeds, has until recently (Xia *et al.*, 2005) remained experimentally unexplored. In this section we elaborate on the results of this experimental investigation and we discuss their implications in relation to the theoretical concept of a ‘preferred’ rupture direction in the presence of bimaterial contrast.

The recent large earthquakes (1999 Izmit and Düzce) and the seismic migration history along the North Anatolian Fault may represent a unique field example of the effect of the material contrast across the fault. The 1999 Izmit and Düzce events featured both supershear and sub-Rayleigh rupture branches (Bouchon *et al.*, 2001). Most significantly, they are the last of a series of large ( $M \geq 6.8$ ) earthquakes that have occurred since 1934 in the North Anatolian Fault. These earthquakes have occurred on a rather long and allegedly inhomogeneous fault system (Zor *et al.*, 2006; Le Pichon *et al.*, 2003) that has hosted tens of major migrating earthquakes in the past century. Following the work of Stein *et al.* (1997) and

of Parsons *et al.* (2000), tens of large ( $M \geq 6.8$ ) earthquakes occurred over 1000 km along the North Anatolian Fault between the 1939 earthquake at Ercinzan and the 1999 Izmit and Düzce earthquakes. Such a long series of earthquakes are believed to be textbook examples of how the transfer of stress from a recent nearby event can trigger the next major event in due time. This presumably happens by adding or transferring stress to the fault segment, which is adjacent to the tips of a segment that has last failed. The stress distribution is highly nonuniform and it occurs in addition to the long-term stress renewal and to the pre-existing stress inhomogeneities. However, as much as this model seems to be complete and convincing, a few questions remain that need to be resolved and are of relevance to the work described here.

#### 4.06.4.1 Two Types of Ruptures along Inhomogeneous Fault Systems

Inhomogeneous faults separate materials with different wave speeds. When such faults experience spontaneous rupture, the equibilateral symmetry, expected in the homogeneous case, is broken. This leads to various forms and degrees of rupture directionality. Dynamic rupture along bimaterial interfaces is known to involve substantial coupling between slip and normal stress (Ben-Zion, 2001; Rice, 2001; Weertman, 1980). As a consequence, the relative ease or difficulty for a rupture to propagate in a specific direction along a bimaterial interface should be closely related to the degree of mismatch in wave speeds. This phenomenon is also related to the fault's frictional characteristics which play a dominant role in facilitating the phenomenon of normal shear coupling. For bimaterial contrast with approximately less than 35% difference in shear wave speeds (as in the case of most natural faults), generalized Rayleigh waves can be sustained. These waves are waves of frictionless contact propagating at a speed,  $C_{GR}$ , called the generalized Rayleigh wave speed (Rice, 2001).

The 1980 rupture solution by Weertman (1980) involves a dislocation like sliding pulse propagating subsonically with a velocity equal to  $C_{GR}$  along an interface governed by Amonton–Coulomb friction. However, the classical Amonton–Coulomb's description has been shown to be inadequate for addressing fundamental issues of sliding (Ranjith and Rice, 2001), since sliding becomes unstable to periodic perturbations. Instability, in the above sense, implies

that periodic perturbations to steady sliding grow unbounded for a wide range of frictional coefficient and bimaterial properties (Adams, 1995; Renardy, 1992). The growth rate is proportional to the wave number. This issue has been discussed in relation of both homogeneous and bimaterial systems (Rice, 2001). For bimaterial systems and in particular, when generalized Rayleigh waves exist, Ranjith and Rice (2001) demonstrate that unstable periodic modes of sliding appear for all values of the friction coefficient. Mathematically, instability to periodic perturbations renders the response of a material interface to be ill-posed (no solution exists to the problem of growth of generic, rather than periodic, self-sustained perturbations to steady sliding). The problem is regularized by utilizing an experimentally based frictional law (Prakash and Clifton, 1993), in which shear strength in response to an abrupt change in normal stress evolves continuously with time (Cochard and Rice, 2000; Ranjith and Rice, 2001). In such a case, the problem becomes well-posed and generic self-sustained pulse solutions exist while numerical convergence through grid size reduction is achieved (Cochard and Rice, 2000; Coker *et al.*, 2005). However, despite the fact that this special frictional law provides regularization, self-sustained slip pulses may still grow in magnitude with time. This is a phenomenon that has been demonstrated numerically by Ben-Zion and Huang (2002). Moreover, self-sustained pulses were found to exist and to propagate at discrete steady velocities and at specific directions along the inhomogeneous interface by analytical (Ranjith and Rice, 2001) and numerical means (Andrews and Ben-Zion, 1997; Cochard and Rice, 2000).

Two types of such steady, self-sustained pulses were discovered by Ranjith and Rice (2001) theoretically. Consistent with Weertman's analysis (Weertman, 1980), the first type corresponds to rupture growth in the direction of sliding of the lower wave speed material of the system. This direction is referred to in the literature (Ben-Zion, 2001; Rice, 2001) as the 'positive' direction and sometimes as the 'preferred' direction (Ben-Zion, 2001). The rupture pulses belonging to this type are subshear and always propagate with a steady velocity  $V = +C_{GR}$ , where the plus denotes growth in the 'positive' direction. Thus, in this work these rupture pulses will be referred to as 'positive' generalized Rayleigh ruptures and will be abbreviated as '+GR' ruptures. The second type of self-sustained rupture corresponds to growth in the direction opposite to that of

sliding in the lower wave speed material of the bimaterial system. This direction is often referred to as the ‘negative’ direction or ‘opposite’ direction (Cochard and Rice, 2000). Such ruptures are supershear and they always propagate with a steady velocity that is slightly lower than the P-wave speed of the material with the lesser wave speed ( $V = -C_p^2$ ). Such ruptures are generated for sufficiently high values of the coefficient of friction (Ranjith and Rice, 2001) and are less unstable than the ‘+GR’ ruptures described above (Cochard and Rice, 2000). In the present paper such ruptures will be abbreviated as ‘ $-P_{\text{SLOW}}$ ’ ruptures. This second type of rupture was later studied by Adams (2001), who showed that the leading edges of these supershear (inter-sonic) ruptures are weakly singular, a result which is consistent with numerical analysis (Cochard and Rice, 2000).

From the point of view of numerics, the early work of Andrews and Ben-Zion (1997) has brought to light the persistence and interesting properties of rupture pulses of the ‘+GR’ type. This was possible even in the ill-posed context of sliding governed by Amontons–Coulomb friction before much of the theoretical concepts were at hand. In their work, the sliding ‘+GR’ pulses were triggered by a local release of interfacial pressure spread out over a finite region at the interface and over finite time. No pulses of the second type (‘ $-P_{\text{SLOW}}$ ’ pulses) were excited in these early simulations despite the fact that the coefficient of friction was high enough to have permitted their existence as suggested by the modal analysis of Ranjith and Rice (Cochard and Rice, 2000). Perhaps this is not altogether surprising if one considers the fact that in these early simulations, nucleation was achieved by a ‘biased’ localized stress drop having a favored propagation direction. In particular, the ‘positive’ direction of growth was artificially seeded in the nucleation process (Ben-Zion, 2006). The subsequent numerical simulations of Cochard and Rice (2000), which utilized the modified Prakash and Clifton Law, still featuring a constant coefficient of friction, were able to sequentially excite regularized self-sustained pulses of both types. This was achieved by introducing small changes in the parameters of the friction law and in the geometry of the nucleation zone. At the same time, no simultaneous excitation of both modes was reported. Moreover, the ‘ $-P_{\text{SLOW}}$ ’ pulses were found to be slightly more difficult to excite than the ‘+GR’ pulses. However, the degree of relative difficulty was not examined in detail. In partial agreement to the above 2-D numerical studies, Harris and Day (1997) demonstrated the

simultaneous existence of both types of sliding modes, propagating in opposite directions during the same rupture event. They considered various bimaterial and trilayered configurations featuring modest wave speed mismatch and a slip-weakening frictional law. As first pointed out by Xia *et al.* (2005), the inconsistency between the various numerical studies is most probably due to the different friction laws utilized. Indeed, up to very recently, all studies except this of Harris and Day (1997) have assumed a constant coefficient of friction. The need for experimental analysis becomes clear at this point since only experiments can be used to judge the physical relevance of various assumed friction laws and to validate various proposed numerical methodologies. As emphasized by Xia *et al.* (2005), the goal of some of the early theoretical and numerical studies (Adams, 1995, 1998; Andrews and Ben-Zion, 1997; Cochard and Rice, 2000; Ranjith and Rice, 2001; Weertman, 1980) was to investigate what kind of unstable slip would develop on a surface which, as judged from conventional friction notions, was superficially stable, in the sense that its friction coefficient,  $\mu$ , did not decrease, or vary otherwise, with slip and/or slip rate. For most brittle solids, however, ample evidence exists that,  $\mu$  does decrease with increase of slip and/or slip rate (or, more fundamentally,  $\mu$  varies with slip rate and contact state). As a result, a proper model for natural faulting along a bimaterial interface should include both a weakening of  $\mu$  and the slip-normal stress coupling effects of the bimaterial situation. Indeed, various models for  $\mu$  are expected to strongly influence the effectiveness of the bimaterial contrast in either enhancing or retarding rupture growth. Such a weakening model was first included by Harris and Day (1997) in a bimaterial context. Given the above, Xia *et al.* (2005) first pointed out that it would be an invalid interpretation of the results of the earlier set of papers (Adams, 1995, 1998; Andrews and Ben-Zion, 1997; Cochard and Rice, 2000; Ranjith and Rice, 2001; Weertman, 1980) to conclude that the rupture scenarios (including preference for specific rupture mode) which they predict constitute the full set of possibilities available to a real earthquake, of which  $\mu$  decreases with increasing slip and/or slip rate. Indeed, according to Xia *et al.* (2005) the consistently bilateral nature of rupture predicted by Harris and Day (1997) is an indication of the effect of including a strongly slip-weakening frictional law in their calculations. In addition, recent refined calculations by Harris and Day (2005) have reconfirmed their conclusions

within a fully 3-D setting. These conclusions, however, have recently been partially challenged by Shi and Ben-Zion (2006) on the basis of an extensive parameter study. A more complete analysis of this on-going discussion will be presented in Section 4.06.4.5.

In the immediately following section, we elaborate on recent experiments (Xia *et al.*, 2005) designed to investigate some of the issues discussed above. We also briefly summarize the recent debate on the existence or nonexistence of a preferable rupture direction which has been triggered by these experiments.

#### 4.06.4.2 Experimental Setup

The experiments described in this section mimic natural earthquake rupture processes in fault systems, where bimaterial contrast between intact rock masses seldom feature more than a 30% difference in shear wave speeds (Rice, 2001).

The laboratory fault model is similar to the one described in Figure 1(a) and is shown in Figure 12. The figure shows a Homalite-100 plate (material 1, top) and a polycarbonate plate (material 2, bottom) that are held together by far-field load,  $P$ . The higher wave speed material at the top (Homalite-100) has a

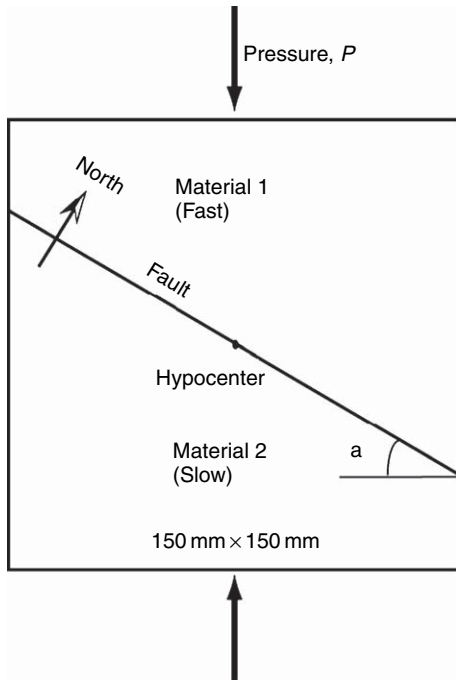


**Figure 12** Laboratory earthquake fault model composed of two photoelastic plates of the same geometry.

shear wave speed  $C_s^1 = 1200 \text{ m s}^{-1}$  and a longitudinal wave speed  $C_p^1 = 2498 \text{ m s}^{-1}$ . The lower wave speed material at the bottom (Polycarbonate) has a shear wave speed  $C_s^2 = 960 \text{ m s}^{-1}$  and a longitudinal wave speed  $C_p^2 = 2182 \text{ m s}^{-1}$ . The fault is simulated by a frictionally held contact interface forming an angle to the applied load that is varied to mimic a wide range of tectonic load conditions. Spontaneous rupture is triggered at the hypocenter through the exploding wire mechanism described in Chapter 1.02. The static compressive load  $P$  is applied through a hydraulic press. By arbitrary convention, the fault line runs in the east–west direction with the lower wave speed solid located at the south side. This choice was motivated in order to eventually facilitate comparisons with the 1999 Izmit earthquake in Turkey. According to the work of Le Pichon *et al.* (2003), the material to the south of the North Anatolian Fault (at its western end near the sea of Marmara) is the lower wave speed solid. As viewed from the camera, a rupture will produce right lateral slip.

The ratio of shear wave speeds,  $C_s^1/C_s^2 = 1.25$ , was chosen to be within the naturally occurring bimaterial range so that the interfacial phenomena can be applied to some field observations. In particular, the bimaterial difference is big enough to allow for a high-enough growth rate of sliding instabilities (Rice, 2001) and to permit the clear distinction between various wave speeds. Within roughly the same range generalized Rayleigh waves exist as well. The shear wave speeds were directly measured for each material by following the shear wave fronts through high-speed photography and photoelasticity. The listed  $P$  wave speeds were calculated by using measured values of Poisson's ratios ( $\nu^1 = 0.35$ ,  $\nu^2 = 0.38$ ) and by using the listed shear wave speeds. An independent measurement of the  $P$ -wave speeds in the plates using ultrasonic transducers confirmed these listed values to within 5%. The value of  $C_{GR}$  can be determined (Rice, 2001) from the equation:

$$f(V) = (1 - b_1^2) a_1 G_2 D_2 + (1 - b_2^2) a_2 G_1 D_1 = 0$$

where  $a_n = \sqrt{1 - V^2 / (C_p^n)^2}$ ,  $b_n = \sqrt{1 - V^2 / (C_s^n)^2}$ ,  $D_n = 4a_n b_n - (1 - b_n^2)^2$ ,  $V$  is the rupture speed,  $G_n$  are rigidities of the two materials, and  $n = 1, 2$ . Substituting the material constants for Homalite-100 and Polycarbonate into the equation, the generalized Rayleigh wave speed is calculated as  $C_{GR} = 950 \text{ km s}^{-1}$ . This is a value that is extremely close to the shear wave speed of Polycarbonate.

#### 4.06.4.3 Experimental Results

More than 30 experiments featuring different angles,  $\alpha$  ( $20^\circ$ ,  $22.5^\circ$ , and  $25^\circ$ ), and far-field loading,  $P$  (10–18 MPa), were performed and the repeatability of rupture events was confirmed. The higher level of angles was limited by the static frictional characteristics of the interface. Depending on  $P$  and  $\alpha$ , three distinct and repeatable rupture behaviors were observed. In all cases, the two separate, semicircular traces of the shear waves in the two materials were clearly visible as discontinuities in the maximum shear stress field. The ruptures were always bilateral and became progressively asymmetric with time, within the time window of all experiments. As shown in **Figure 13**, two distinct rupture tips, one moving to the west and the other moving to the east, with velocities  $V_E$  and  $V_W$ , respectively, were identified by a distinct concentration of fringe lines. For this case (case-1), both tips propagate at subshear velocities  $V_E < V_W < C_S^2 < C_S^1$ . Differentiation of the rupture length–time histories, obtained from a series of high-speed images, allows for the estimation of the rupture velocity histories. On the one hand, the rupture moving to the west is the one propagating in the direction of sliding of the lower wave speed material (positive direction). Within experimental error this rupture was found to grow at a constant velocity equal to the speed of the generalized Rayleigh waves ( $V_W = 950 \text{ m s}^{-1} \approx +C_{GR}$ ). The rupture moving to the east, on the other hand, was the one propagating

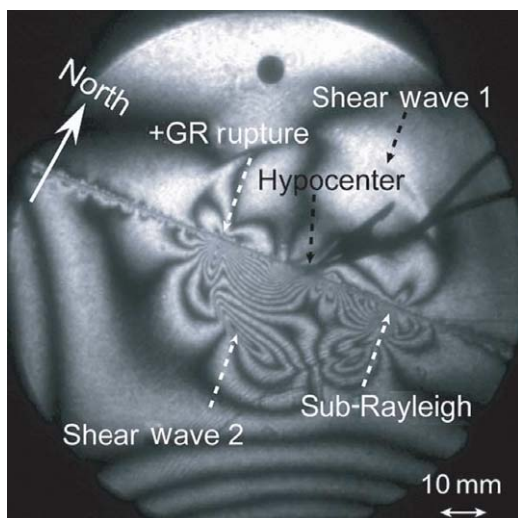


**Figure 13** The photoelastic patterns for an experiment with  $\alpha = 22.5^\circ$ ,  $P = 17 \text{ MPa}$ , and smooth surface. Both ruptures to the east and the west are subshear (case-1).

in the direction opposite to that of sliding in the lower wave speed material (opposite direction). This rupture grew at an almost constant sub-Rayleigh velocity of  $V_E = -900 \text{ m s}^{-1}$ , which is clearly slower than the Rayleigh wave speed,  $C_R^2$ , of the slower wave speed material. The observations were very similar for smaller angles,  $\alpha$ , and compressive loads,  $P$ , as well. The rupture to the west (positive direction) always propagated with  $+C_{GR}$ . The rupture to the east remained sub-Rayleigh ( $V_E < C_R^2 < C_R^1$ ). However, its velocity varied across experiments with different load levels and angles. In particular, smaller angles of  $\alpha$  (or smaller values of the  $s$  factor described earlier) and lower  $P$  resulted in  $V_E$  being lower fractions of  $C_R^2$ . Judging from the number of near-tip fringes per unit area, the eastward moving rupture resulted in a visibly smaller level of stress drop than the one moving to the west. This observation is consistent with predictions by [Cochard and Rice \(2000\)](#) and [Adams \(2001\)](#) who also predict a weaker singularity for ruptures moving in the negative direction.

A very distinct but equally repeatable rupture case (case-2) was observed for higher values of  $\alpha$  and  $P$ . These conditions correspond to much higher values of driving stress or to conditions closer to incipient uniform sliding of the entire interface (smaller values of  $s$ ). A typical example corresponding to  $\alpha = 25^\circ$  and  $P = 17 \text{ MPa}$  is shown in **Figure 14**. In this case the rupture is still bilateral with a westward tip trailing

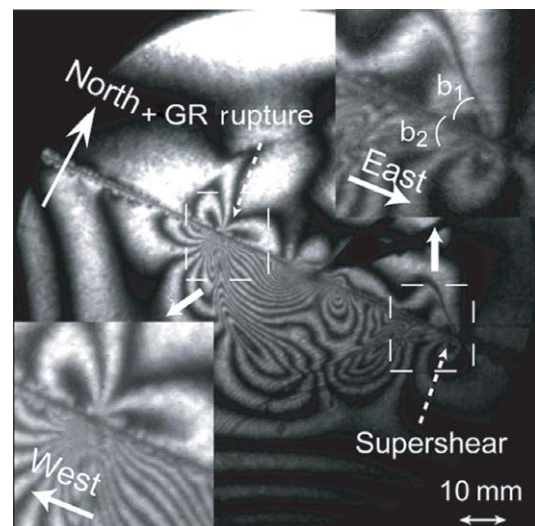


**Figure 14** For  $\alpha = 25^\circ$ ,  $P = 17 \text{ MPa}$ , and smooth surface finish the bilateral rupture features two distinct tips. The one moving to the west (positive direction) has a velocity  $V_W \approx +C_{GR}$ , while the one moving to the east (opposite direction) is supershear. (case-2).

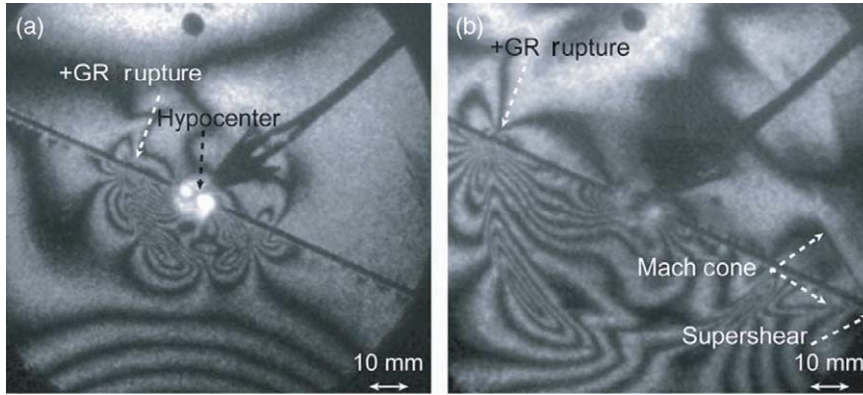


**Figure 15** Experimental results for  $\alpha = 25^\circ$ ,  $P = 13$  MPa, and rough surface showing transition of the eastward moving rupture to supershear. The westward rupture retains a constant velocity  $V_W \approx +C_{GR}$  (case-3).

behind both shear wave traces. This tip moves at a constant velocity  $V_W \approx +C_{GR}$  along the ‘positive’ direction. This observation is identical to the situation described above in relation to lower values  $\alpha$  and  $P$ . The eastward moving tip however is clearly different from the previously described case. Its tip is moving with a velocity faster than both the shear wave speeds. Moreover, its structure, shown in detail in the upper inset of **Figure 14**, is distinctly different to the structure of the sub-Rayleigh, westward moving rupture shown in the lower inset.

As conclusive proof of its supershear velocity, two distinct shear shock waves are clearly visible. The magnitude of the velocity of the eastward rupture  $V_E$  is  $1920 \text{ m s}^{-1}$ , which is approximately 12% less than the P-wave speed,  $C_P^2$ , of the lower wave speed material.  $V_E$  is also equal to  $1.6 C_S^1$ , or is slightly higher than  $\sqrt{2} C_S^1$ . The upper inset in **Figure 14** shows two clear lines of discontinuity in the maximum shear contours of photoelasticity. Each of these lines (shear shock waves) is located at two different angles  $\beta_1 = 41^\circ$  and  $\beta_2 = 30^\circ$ , to the north and to the south of the fault respectively. The two angles  $\beta_n$  ( $n = 1, 2$ ) are related to the shear wave speeds  $C_S^n$  and to the rupture velocity  $V_E$ , by  $\beta_n = \sin^{-1}(V_E/C_S^n)$ . This relation provides independent means of estimating  $V_E$  from each individual frame of the high-speed camera record without reliance on the less accurate rupture length history. Both methods yield consistent values of  $V_E = -1920 \text{ m s}^{-1}$ .

Both cases described above feature westward moving ruptures that are of the ‘+GR’ type. Irrespective of the values of  $\alpha$  and  $P$ , these ruptures have a constant speed  $V_W \approx +C_{GR}$ , and they propagate in the ‘positive’ direction. However, those two cases also feature eastward ruptures that are distinctly different in nature. For

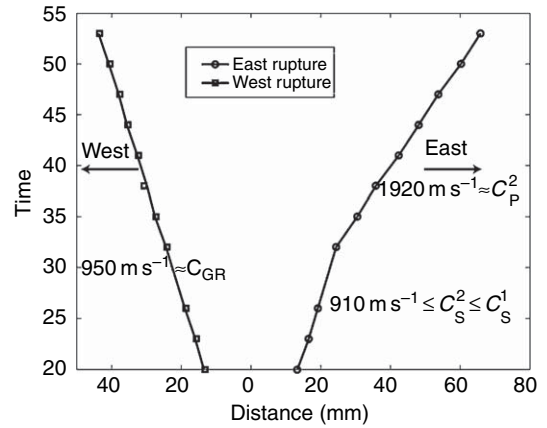


**Figure 16** Rupture length plot of an experiment for  $\alpha = 25^\circ$ ,  $P = 13$  MPa, and rough surface finish.

sufficiently low  $P$  and  $\alpha$  (or large  $s$ ), the eastward ruptures, which propagate in the opposite direction, are purely sub-Rayleigh within the time window of our experiments. For large-enough  $P$  and  $\alpha$  however, eastward ruptures propagate in the opposite direction with a constant supershear velocity, which is slightly less than  $C_P^2$  and are thus of the ‘ $-P_{SLOW}$ ’ type.

To visualize an intermediate situation and a controlled transition from one case to the other within the field of view,  $P$  was reduced to 13 MPa. For this case (case-3), **Figure 15** shows a smooth transition from case-1 to case-2 within the same experiment. While the westward rupture remains of the ‘+GR’ type throughout the experiment, the eastward rupture jumps from a constant sub-Rayleigh velocity ( $-910 \text{ m s}^{-1}$ ) to a constant supershear velocity ( $-1920 \text{ m s}^{-1}$ ), and thus transitions to the ‘ $-P_{SLOW}$ ’ type. The rupture length plot of **Figure 16** also

shows the abrupt transition of the eastward rupture from a sub-Rayleigh velocity to a velocity slightly less than  $C_p^2$ . This happens at a transition length,  $L$ , which is approximately equal to 25 mm. However, the westward rupture retains its constant  $+C_{GR}$  velocity throughout the experiment. The eastward transition behavior of case-3 is qualitatively similar to the one we have discussed in relation to homogeneous interfaces (Xia *et al.*, 2004), while the transition length,  $L$ , is also a decreasing function of  $\alpha$  and  $P$ . Most important to the discussion of the present paper is the observation that the ruptures that propagate to the opposite direction require a certain minimum rupture length before they become supershear. This observation provides a clear intuitive link between super shear growth in the ‘opposite’ direction and large earthquakes. In contrast, no such transition was observed for ‘positively’ growing ‘+GR’ ruptures irrespective of  $\alpha$ ,  $P$ , and rupture length. As a result, the experiments do not provide an obvious link between ‘positively’ growing ruptures and large earthquakes.

In other words, a certain minimum length of rupture growth in the negative direction is required before such a transition can be observed. This suggests that in smaller earthquake events, such as the 2004 Parkfield rupture such a transition may not have had the chance to happen before the negative moving rupture was arrested. (for more on Parkfield, see Section 4.06.4.5).

In Section 4.06.3.3, we have discussed the dependence of the transition length  $L$  on the uniaxial pressure  $P$ . In the homogeneous case there is a very well-defined point for transition, while in the inhomogeneous case the transition point is not always so clear. This difference again is due to the presence of a material contrast. In the homogeneous case, there is an energetically forbidden velocity zone between  $C_R$  and  $C_S$  (Rosakis, 2002). As a result, the secondary crack is initiated exactly at the shear wave front. In contrast for inhomogeneous fault systems, the forbidden zone no longer exists (Rosakis, 2002) and the subshear crack in the opposite direction accelerates to the supershear speed in a smoother way (Figure 16). Nevertheless, we can still define the transition length where a rapid speed change occurs. The plot of transition length  $L$  is in Figure 17.  $L$  has a weaker dependence on  $P$  ( $L \sim P^{-0.4}$ ) than the homogeneous case ( $L \sim P^{-1.5}$ ). This is expected because for the inhomogeneous case, and for subshear rupture speeds, the coupling between the slip and the normal traction causes a local rupture-tip compression. This

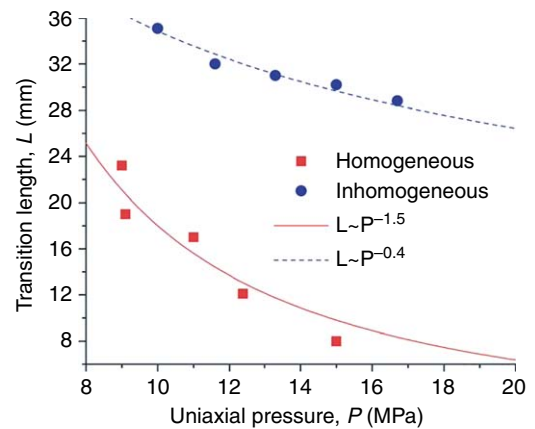


**Figure 17** Transition length as a function of pressure  $P$  for experiments with  $\alpha = 25^\circ$ . The data and fitting curves for the homogeneous case are included for comparison.

compression increases the resistance to slip for rupture growing in the negative direction. On the other hand, the shear traction driving the rupture is constant and hence it takes a longer slip distance for a rupture in bimaterial interface to reach the super-shear velocity.

#### 4.06.4.4 Comparison of the Experimental Results to Early Numerical and Theoretical Studies

The experiments by Xia *et al.* (2004, 2005) described above provide the first full-field and real-time visualization of dynamic frictional rupture events occurring along inhomogeneous interfaces, which feature low-wave-speed mismatch such that the generalized Rayleigh wave speed can be defined. While it is very difficult to access whether the ruptures are pulse-like, crack-like, or a mixture of the two, the observations confirm the existence of two distinct self-sustained and constant speed rupture modes. These bare strong similarities to the ones that have been theoretically and numerically predicted over the recent years (Andrews and Ben-Zion, 1997; Ben-Zion, 2001; Ben-Zion and Huang, 2002; Cochard and Rice, 2000; Rice, 2001; Weertman, 1980). In particular, a ‘+GR’ type of rupture mode is always excited instantaneously along the ‘positive’ direction of sliding. Besides the ‘+GR’ rupture mode, a ‘ $-P_{SLOW}$ ’ mode is observed as long as the rupture propagating in the ‘opposite’ direction is allowed to grow to sufficiently long distances from the hypocenter. The triggering of the ‘ $-P_{SLOW}$ ’ mode is always preceded by a purely sub-Rayleigh, crack-like

rupture whose velocity depends on loading, on geometry, and on the bimaterial characteristics. Therefore, the existence of this preliminary and apparently transient stage is one of the main differences with the early numerical predictions (Andrews and Ben-Zion, 1997; Cochard and Rice, 2000). However, its existence does not contradict early theoretical studies (Adams, 2001; Ranjith and Rice, 2001), which can only predict stable rupture events whose constant velocities relate to the wave speeds of the bimaterial system.

A far more striking difference to some of the early numerical predictions (Andrews and Ben-Zion, 1997; Ben-Zion and Huang, 2002; Cochard and Rice, 2000) is the consistent experimental observation of bilateral slip. In contrast to the experiments, the above numerical predictions seem capable only of exciting one or the other of the two self-sustained rupture modes (Cochard and Rice, 2000), giving rise to purely unilateral rupture events. They also seem to primarily favor the triggering of the '+GR' mode in low-wave-speed mismatch bimaterial systems (Andrews and Ben-Zion, 1997). This kind of preference has led to the labeling of the 'positive' direction as the 'favored' rupture direction and of  $+C_{GR}$  as the 'favored' rupture velocity. These numerical results indirectly support the closely related notion of ruptured directionality (McGuire *et al.*, 2002). A notable exception to this rule is provided by the early numerical analysis by Harris and Day (1997), as well as their subsequent work (Harris and Day, 2005; Andrews and Harris, 2005) which consistently reports asymmetric bilateral rupture growth in a variety of low-speed contrast, inhomogeneous fault systems. These results are qualitatively very similar to the experimental observations of cases 1 and 2. In particular, the latter 3-D results by Harris and Day (2005) also clearly report on sub-Rayleigh to supershear transition for the rupture propagating along the negative direction. As briefly discussed by Cochard and Rice (2000) and Xia *et al.* (2005), the excitation of various modes or their combinations should be related to the details of the numerically or experimentally implemented triggering mechanisms. In an attempt to further reconcile the observed differences between various models and the experiments, Xia *et al.* (2005) have noted that unstable slip rupture propagation has also been observed (Xia *et al.*, 2004) on homogeneous Homalite/Homalite and Polycarbonate/Polycarbonate interfaces. Such unstable rupture growth would be possible only if there was a substantial reduction of the friction coefficient with slip and/or slip rate, and hence such reduction must be a property of both these model materials when sliding

against each other. It is then plausible to assume that a similar reduction of friction coefficient occurs along the Homalite/Polycarbonate interface, and to thus infer that its rupture behavior should not be expected to fully correspond to the idealized models of a dissimilar material interface with constant coefficient of friction (Adams, 1995, 1998; Andrews and Ben-Zion, 1997; Cochard and Rice, 2000; Ranjith and Rice, 2001; Weertman, 1980). Indeed, the stronger the weakening becomes, the reduced frictional resistance is expected to further neutralize the effect of bimaterial contrast on normal shear coupling thus rendering the 'preferable' rupture direction less preferable than originally thought.

The present experiments neither support exclusivity nor show a strong preference for rupture direction. Although they support the idea that frictional ruptures that grow in the positive direction will always do so at a specific constant velocity ( $V = +C_{GR}$ ), they still allow for a significant possibility of self-sustained supershear ruptures growing in the opposite direction. This possibility becomes significant, provided that their transient, sub-Rayleigh precursors grow for a large-enough length and are not arrested prior to transitioning to supershear. The requirement of a critical transition length along the 'opposite' direction provides a link between large earthquakes and the occurrence of self-sustained supershear rupture in the 'opposite' direction. One perhaps can contemplate the existence of a weak statistical preference for positively growing ruptures, since this link to large earthquakes is absent for '+GR' ruptures.

#### 4.06.4.5 The Parkfield Earthquake Discussion in the Context of Experiments and of Recent Numerical Studies

The Parkfield earthquake sequence presents a very interesting case in the context of bimaterial rupture and the issue of the existence, or lack of, a preferable rupture direction. The slip on the San Andreas Fault is right-lateral, and the crust, near Parkfield, on the west side of the fault features faster wave speeds than the east side (Thurber *et al.*, 2003). The three most recent major Parkfield earthquakes ruptured the same section of the San Andreas Fault. The rupture directions of the 1934 and the 1966 events were southeastward (positive direction), whereas the 2004 earthquake ruptured in the opposite direction (negative direction). Following the discussion above, results from the early constant friction coefficient

studies in bimaternal would imply that the positive (southeastward) direction of the 1934 and the 1966 events is the preferable direction. According to this notion, the negative (northwestward) direction of the 2004 earthquake would not be favored. The experiments described above (Xia *et al.*, 2005), however, have clearly demonstrated that a rupture in the negative direction can indeed occur at least in model materials. Such a rupture, depending on tectonic loading conditions and on available rupture length, may grow at either sub-Rayleigh or at supershear rupture speeds. Motivated by the most recent 2004 Parkfield event and supported by the Xia *et al.* (2005), Harris and Day (2005) extended their earlier 1997 work to three dimensions and discussed their results in relation to extensive observational evidence collected from the past 70 years of earthquakes at the vicinity of Parkfield. They concluded that natural earthquake rupture propagation direction is unlikely to be predictable on the basis of bimaternal contrast.

The scientific discussion on the notion of rupture directionality is however far from being over. In a recent paper, Shi and Ben-Zion (2006) have presented an extensive parameter study for various bimaternal contrasts which clearly shows the effect of assumed frictional properties and nucleation conditions in promoting either unilateral (preferred) or bilateral (nonpreferred) rupture in the presence of bimaternal contrast. Their study utilized a classical linear slip-weakening model of friction of the same type used by Harris and Day (1997, 2005). It shows that for small differences  $\mu^s - \mu^d \sim 0.1$  between the static and dynamic coefficient of friction and for nonbiased nucleation events, the bimaternal effect indeed induces ruptures which primarily grow in the positive direction at  $+C_{GR}$ . These cases are consistent with the constant coefficient friction models. However, when the difference between the two coefficients of friction is taken to be larger than or equal to 0.5 and for 20% shear wave speed contrast, bilateral rupture in both directions becomes possible with speeds equal to  $+C_{GR}$  in the positive direction, and depending on the nucleation condition, with either subshear or supershear ( $-P_{SLOW}$ ) speeds in the negative direction. These cases are consistent with the experiments and perhaps with the Parkfield observations. Their results also agree with the above-discussed explanation, originally offered by Xia *et al.* (2005), regarding the root cause of the differences between the experimental results and the prediction of a preferable direction in the early numerical studies. Indeed the difference of friction coefficient in

the experiments is expected to be in the range of 0.4–0.5 (see Section 4.06.2.2.3 for the homogeneous case) which, within the slip weakening assumption, would promote bilateral ruptures of various types. Moreover, this recent study does not conclusively settle the issue of rupture direction preference in natural earthquakes where frictional characteristics are generally unknown. Nevertheless it clearly shows that the main arbitrator in whether bimaternal contrast is capable of inducing rupture directionality, through normal to shear coupling, is the frictional law. Clearly, much more work is needed to investigate this phenomenon. The inclusion of realistic frictional laws including strong velocity weakening or enhanced rate and state frictional descriptions which regularize the rupture problem could be a first step. Another step would necessitate the numerical and experimental study of a variety of bimaternal contrasts and of more naturally based nucleation conditions. Nucleation conditions are shown by Lu *et al.* (2005) (homogeneous case) and by Shi and Ben-Zion (2006) and Rubín and Ampuero (2006) (inhomogeneous case) to have a strong influence on subsequent rupture growth. We believe that transition lengths for example may be heavily dependent on nucleation conditions. The recent papers by Andrews and Harris (2005) and Ben-Zion (2006), as well as the work of Rubín and Ampuero (2006) are also very important recent references reflecting the on-going discussion on this subject.

#### 4.06.4.6 Discussion of the Historic, North Anatolian Fault Earthquake Sequence in View of the Experimental Results

The 1999, M7.4, Izmit earthquake in Turkey is perhaps a prime example of a recent large earthquake event for which both modes of self-sustained rupture may have been simultaneously present, as is the case in our experiments. The event featured right-lateral slip and bilateral rupture of a rather straight strike-slip segment of the North Anatolian Fault shown in Figure 18. As reported by Bouchon *et al.* (2001), the westward propagating side of the rupture grew with a velocity close to the Rayleigh wave speed, while the eastward moving rupture grew at a supershear velocity that was slightly above the  $\sqrt{2}C_S$  times the shear wave speed of crustal rock. The visible difference in the nature of the seismographs from stations ARC and SKR situated almost equidistantly to the hypocenter (star) support their conclusion (see bottom of Figure 18). Since the laboratory ruptures of the

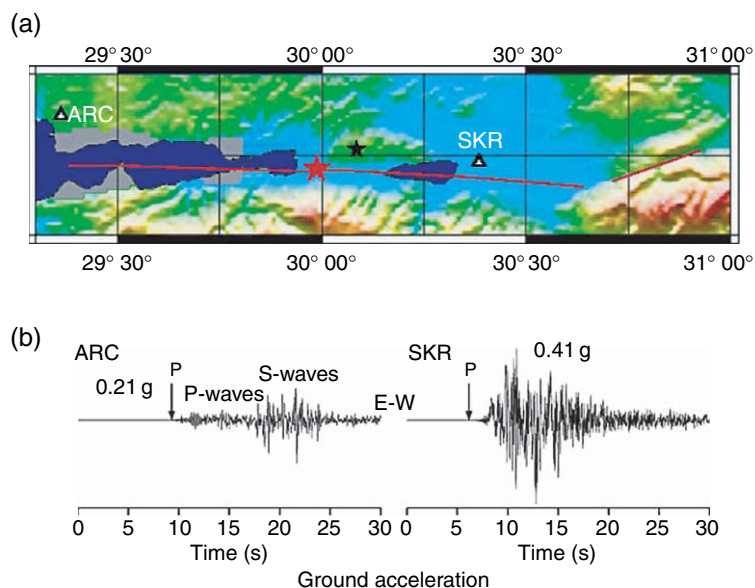


**Figure 18** (a) Map view indicating the hypocenter of 1999 Izmit earthquake and two seismological stations ARC and SKR; (b) Seismograms obtained at ARC and SKR. Reproduced from Bouchon M, Bouin MP, Karabulut H, Toksoz MN, Dietrich M, and Rosakis AJ (2001) How fast is rupture during an earthquake? New insights from the 1999 Turkey earthquakes. *Geophysical Research Letters* 28(14); 2723–2726.

current paper are intentionally oriented similarly to the Izmit event (lower-wave-speed material to the south as indicated by Le Pichon *et al.*, 2003), a direct comparison with the case described in Figure 14 becomes possible and it reveals some striking similarities between Bouchon *et al.*, (2001) interpretation of the earthquake and the experiment. In addition to featuring right lateral slip and asymmetric bilateral rupture, this experimental case (case-2) featured a subshear westward rupture propagating at  $+C_{GR}$ . To the east however, the rupture propagated at a velocity slightly lower than  $C_p^2$ , which also happens to be equal to  $1.6 C_s^1$  for the particular bimaterial contrast of the experiments. If one interprets the Izmit event as occurring in an inhomogeneous fault with the lower-wave-speed material being situated at the southern side of the fault (as is in the experiment), the field observations and the experimental measurements of both rupture directions and velocities are very consistent. Moreover, when the bimaterial contrast is low enough, the differences between  $C_{GR}$  and the average of the two Rayleigh wave speeds,  $(C_R^1 + C_R^2)/2$ , as well as the difference between an inferred rupture speed of  $1.6 C_s^1$  and  $\sqrt{2}(C_s^1 + C_s^2)/2$  would be small enough not to be discriminated by the inversion process, even if the fault geology was completely known. In this respect, the agreement with experiment is as good as it can ever be expected. In

addition, viewing the fault as inhomogeneous can explain the choice of direction for both the sub-Rayleigh and the supershear branches, respectively. This choice of rupture direction is consistent with both the present experiments and with the theories reviewed in the introduction.

The 1999 Düzce earthquake can also be interpreted through a similar line of argument used for Izmit. The Düzce rupture also featured right lateral slip (as did all events that occurred in the North Anatolian Fault between 1939 and 1999) and it extended the Izmit rupture zone 40 km eastward (negative direction) through asymmetric bilateral slip (Bouchon *et al.*, 2001). Thus, similar to the Izmit earthquake, numerical modeling by Bouchon *et al.* (2001) indicates both sub-Rayleigh westward and supershear eastward rupture fronts. As a result the direct comparison with case-2 described in Figure 14 provides an explanation for the two rupture directions and respective velocities, similar to the one given for Izmit. This explanation is of course plausible only if one assumes, once again, that the material to the south of the North Anatolian Fault (at its western end) is the lower-wave-speed solid. Strong evidence supporting this assumption has recently been presented by Le Pichon *et al.* (2003).

By using similar arguments to the ones used for Izmit and Düzce, one can perhaps attempt to provide

a unified rationalization of the seemingly random rupture directions and rupture velocities of the inter-related series of earthquakes that occurred since 1939 along the North Anatolian Fault and ended in 1999 with the Izmit and Düzce events. The following argument requires the assumption that, in average and along its entire length, the North Anatolian Fault features the same type of bimaterial in-homogeneity as the one that has been summarized for Izmit and Düzce. However, rather limited evidence supporting such an assumption is currently available (Zor *et al.*, 2006). If in some average sense this is true, one would expect that the slight majority (60%) of the large ( $M \geq 6.8$ ) earthquake events (i.e., (1939-M7.9), (1942-M6.9), (1944-M7.5), (1951-M6.8), (1957-M6.8), (1967-M7.0)) which featured westward growing ruptures, were probably of the '+GR' type. In other words, this assumption implies that they were classical sub-Rayleigh ruptures that moved with velocity equal to  $+C_{GR}$  in the 'positive' direction. The remaining ruptures of the series were 'special' in the sense that they featured dominant eastward growth. As previously detailed, out of the remaining four ruptures of the series, the Izmit and Düzce events were bilateral with a western branch of the '+GR' type (consistent with the others) and an eastward, supershear branch of the '- $P_{SLOW}$ ' type. The 1943 and 1949 ruptures were purely unidirectional and eastward moving; however, their rupture velocities are not known. If these ruptures are to be consistent with the remaining events in the sequence then they could also have developed as the '- $P_{SLOW}$ ' type. This possibility is more likely for the 1943 event that featured over 250 km of growth length. As estimated in Section 4.06.2.2.3, this length is much larger than the critical length required for transition to supershear. By observing that the 1943 and the two 1999 (Izmit and Düzce) events were of a higher magnitude than most of the other events of the complete series, as reported by Stein, *et al.* (1997), further supports the assertion that at least three out of four 'special' events featured partial or total supershear growth along the 'opposite' (eastward) direction. The basic support for this assertion is provided by the experimentally established link between large earthquakes and supershear ruptures growing in the 'opposite' direction, and is consistent with the direct evidence of supershear from the two most recent 'special' events of 1999.

Finally, it should be noted that if earthquakes of lesser magnitude (in the range between M6.4–6.8) are also included in the discussion, the North Anatolian

Fault series will feature a weak preference for western propagation. This is not very surprising given the above discussed link between large earthquakes and self-sustained supershear along the opposite direction, a link that does not exist for 'positive' (westward growing) '+GR' ruptures. Indeed, in addition to the actual number of ruptures that grew to the east or west, what is of importance here is the actual growth lengths. The results reported by Stein *et al.* (1997) show that the total length of westward growth is only slightly higher than that of eastward growth. This is again consistent with experiments which show that the self-sustained '+GR' mode is always and instantaneously present after nucleation. In contrast, the self-sustained '- $P_{SLOW}$ ' mode is often preceded by an unstable subshear phase. For smaller earthquakes this unstable phase may never transition to supershear and instead it may be arrested. This in turn would result in a total eastward rupture length, which is slightly shorter than the total western rupture length of the earthquake series.

#### 4.06.5 Observing Crack-Like, Pulse-Like, Wrinkle-Like and Mixed Rupture Modes in the Laboratory

The duration of slip at a point on an interface (or fault) in comparison to the duration of the rupture of the entire fault is a central issue to the modeling of earthquake rupture. There are two widely accepted approaches to the description of dynamic sliding (Rice, 2001). The most classic approach uses elastodynamic shear rupture (or crack) models in which the surfaces behind the leading edge of the rupture (rupture tip) continuously slide and interact through contact and friction. More recently, pulse-like models in which sliding occurs over a relatively small region have been introduced (Heaton, 1990). In these models, the sliding is confined to a finite length which is propagating at the rupture speed and is followed by interfacial locking.

In faults separating identical materials (homogeneous systems) the crack-like mode of rupture has often (but not exclusively) been generated in many numerical simulations of spontaneous rupture when a rate-independent friction law was implemented (Madariaga, 1976; Andrews, 1976, 1985; Das and Aki, 1977; Day, 1982; Ruppert and Yomogida, 1992; Harris and Day, 1993). It has been pointed out, however, that inversions of seismic data for slip histories, from well-recorded events, indicate that the duration

of slip at a point on the fault is one order of magnitude shorter than the total event duration. An attempt to explain this phenomenon has given rise to the concept of a pulse-like rupture mode (Heaton, 1982, 1990; Hartzell and Heaton, 1983; Liu and Helmlinger, 1983; Mendoza and Hartzell, 1988, 1989). Some eyewitness accounts have also reported short slip durations during some earthquakes (Wallace, 1983; Pelton *et al.*, 1984).

The concept of a pulse-like rupture went against a widely accepted view of how seismic rupture occurs. Its introduction was followed by various efforts to illuminate the physics leading to this process through analytical and numerical investigations. Different mechanisms for 'self-healing' pulse generation along faults in homogeneous systems have been proposed (Heaton, 1990). One postulation is that if the fault strength is low immediately behind the rupture front and is increased rapidly at a finite distance, then slip might be restricted to a short, narrow propagating area (Brune, 1976). Recent theoretical and numerical investigations show that a strong velocity-weakening friction law model could indeed allow for pulse-like behavior of rupture under certain conditions (Zheng and Rice, 1998). However, simulations utilizing velocity weakening have sometimes resulted in crack-like ruptures and sometimes in 'self-healing' pulses (e.g., Cochard and Madariaga, 1994, 1996; Perrin *et al.*, 1995; Beeler and Tullis, 1996; Ben-Zion and Rice, 1997; Lapusta *et al.*, 2000; Cochard and Rice, 2000; Nielsen *et al.*, 2000; Coker *et al.*, 2005). Friction laws along interfaces between two identical elastic solids have to include laboratory-based rate and state evolution features and they must not exhibit illposedness or paradoxical features (Cochard and Rice, 2000; Ranjith and Rice, 2001). It has been proved that generalized rate and state friction laws are appropriate candidates for homogeneous fault systems (Cochard and Rice, 2000; Ranjith and Rice, 2001; Rice *et al.*, 2001; Zheng and Rice, 1998). Within the frame of rate and state friction laws, the following three requirements have to be fulfilled for rupture to occur as a 'self-healing' pulse (Zheng and Rice, 1998; Rice, 2001). One requirement is that the friction law must include strengthening with time on slipped portions of the interface that are momentarily in stationary contact (Perrin *et al.*, 1995). Another is that the velocity weakening at high slip rates must be much greater than that associated with the weak logarithmic dependence observed in the laboratory during low-velocity sliding experiments. This is often termed 'enhanced' velocity weakening. Lastly,

the third requirement is that the overall driving stress has to be lower than a certain value, but high enough to allow for self-sustained pulse propagation (Zheng and Rice, 1998).

While strong velocity weakening is one mechanism which explains the onset of short duration slip-pulses along interfaces (faults) which separate similar materials, it is important to note that other mechanisms exist as well. One involves geometric confinement of the rupture domain by unbreakable regions (barrier model). That is, sliding consists of a number of crack-like ruptures of short duration on a small rupture area that are separated by locked regions (Aki, 1979; Papageorgiou and Aki, 1983a, 1983b). In one implementation of this scenario, a pulse-like rupture behavior was found in a 3-D geometry when the rupture process was confined within a long but narrow region by unbreakable barriers (Day, 1982). It was observed that the rupture starts in a classic crack-like mode and it propagates in all directions. After some time, arresting waves arrive from the boundaries and they effectively relock the fault behind the rupture front, resulting in two slip pulses. Alternatively, a rupture nucleates and propagates bilaterally, but may arrest suddenly at a strong barrier at one end. Following its arrest, the reflected waves from the barrier spread back and heal the rupture surface. The combination of the still-propagating end of the rupture with the healing reflected wave forms a moving pulse-like configuration (Johnson, 1990).

In general, narrow slip pulses can be generated during dynamic sliding along interfaces by strongly velocity-weakening friction on a homogeneous system, by strong fault zone heterogeneities (Rice, 2001) or by variations in normal stress along the rupture interface. All of the above conditions (velocity weakening, heterogeneities, and local normal stress variation) can produce slip pulses with low dynamic stress at the active part of the slip. An extensive discussion of the subject is presented by Nielsen and Madariaga (2003). Most relevant to the discussion here is a set of recent finite element calculations which have been carried out by Coker *et al.* (2005) for a configuration which is very similar to the experimental setup described in the next section. These simulations have shown that it is possible to generate a great variety of dynamic rupture modes (cracks, pulses, and pulse trains) propagating along an interface characterized by a rate-enhanced, rate- and state-dependent frictional law. The choice of rupture speed and rupture mode clearly depends on the load

intensity and rate but it is also very sensitive to the type of constitutive law employed, as well as the values of its parameters.

#### 4.06.5.1 Experimental Investigation of Dynamic Rupture Modes

As discussed in Section 4.06.2.1, the majority of the existing experimental studies on sliding concentrate on processes occurring over large timescales (large compared to wave transit within the specimen) and are concerned with developing relationships between time-averaged friction data and various system parameters. Many dynamic friction laws motivated by using various experimental configurations and apparatus lack the reproducibility of friction data (survey by Ibrahim, 1994) to be of definite value to the theorists. The results of these experiments are multi-branched friction versus slip velocity curves, which even for the same material and the same experimental configuration depend not only on the properties of the frictional interface but also on the dynamic properties of the apparatus, such as mass, stiffness, and damping. This suggests that the friction data obtained in the course of stick-slip motions do not purely reflect the intrinsic properties of the surfaces in contact but are also greatly affected by several of the dynamic variables involved in each particular experimental setup. Another shortcoming of the experiments described above, in relation to their relevance to real earthquakes, is the achievable range of sliding speeds. Typically, natural earthquakes involve sliding velocities on the order of  $1\text{--}10\text{ m s}^{-1}$  while these experiments involve sliding in the range of  $1\text{ }\mu\text{m s}^{-1}$  to  $1\text{ mm s}^{-1}$ . An exception to this rule are the experiments of Prakash and Clifton (1993) and of Prakash (1998), who employed a plate-impact pressure-shear friction configuration to investigate the dynamic sliding response of an incoherent interface in the microsecond timescale (sliding speeds on the order of  $10\text{ m s}^{-1}$ ). The experimental results, deduced from the response to step changes imposed on the normal pressure at the frictional interface, reinforce the importance of including frictional memory in the development of the rate-dependent state variable friction models. However, this setup is essentially 1-D. As such it is not able to provide information about the detailed stress field developed along the length of the interface nor to shed light on the nature (e.g., uniformity or lack of) of the rupture process during dynamic sliding. As in many cases described in Section 4.06.2.1.1, the

implicit assumption crucial to the interpretation of the data is that both stress and sliding processes remain spatially uniform. Another exception is the very recent work by Tullis and his co-workers (Di Toro *et al.*, 2004; Tullis and Goldsby, 2003) who have approached seismic slip rates in experiments involving crustal and quartz rock. They have investigated the phenomenon of flash heating as the main mechanism resulting in severe velocity weakening. They have shown that the phenomenon of flash heating (Rice, 1999) can be experimentally linked to the observed behavior of drastic velocity weakening observed in their experiments. Finally, the scarcity of fast sliding velocity data in the open literature has to be emphasized. We believe that this is an essential data set which could be proved as the ultimate arbitrator for the validation of various dynamic sliding models and friction laws.

Rubinstein *et al.* (2004) conducted experiments to investigate the onset of dynamic sliding. They considered two blocks of PMMA separated by a rough interface and subjected to vertical static compression and to a gradually increased horizontal driving force. During the sliding initiation, they recorded the relative change of the net local contact area as a function of time by measuring the changes of the light intensity transmitted across the interface. The transmitted light was imaged by a camera. Because of the low framing rates of their recording apparatus, their experimental configuration was particularly suited to the study of ‘slow’ phenomena, with respect to the characteristic wave speeds of the material. They discovered slow waves propagating at speeds between  $40\text{ m s}^{-1}$  and  $80\text{ m s}^{-1}$ , which is one order of magnitude slower than the Rayleigh wave speed of PMMA. These detachment waves, which are perhaps related to Schallamach waves, because of their low propagation speeds (Schallamach, 1971), are very important since they give rise to a significant amount of slip. There are some doubts, however, to whether the characteristics of these waves are determined only by the properties of the surfaces in contact and by the loading. Because of their low rupture speeds, it is also likely that the dynamic properties of the entire specimen may play an important role in the formation of these waves. If the above is true, then the slow detachment waves, though very important to sliding of finite bodies, may be less relevant to natural earthquakes. Another very interesting question, which also remains to be answered, is whether these ‘detachment’ waves generate opening at the interface, thus justifying their name.

As it is clear from the experiments presented both in Section 4.06.2.1.1 and above, most of the experimental methods employed up to this point lack the spatial or/and the temporal resolution to address some important questions on dynamic sliding related to the sliding initiation process, to the duration of sliding (or sliding mode), and to the changes in the stress field distribution along the interface. This is particularly true in cases where sliding speeds on the order of  $1 \text{ m s}^{-1}$ , or above, are involved. To remedy this situation, the physical plausibility of generating pulse-like and crack-like rupture modes along ‘incoherent’ (frictional) interfaces in homogeneous systems has been investigated by Lykotrafitis *et al.* (2006a) in a number of well-controlled experiments. The sliding speeds were on the order of  $1 \text{ m s}^{-1}$ . This sliding speed is of the same order of magnitude as the one expected in most ‘large’ natural earthquake rupture events.

Dynamic photoelasticity combined with a new laser interferometry-based technique has provided direct physical evidence of the rupture mode type, the exact point of rupture initiation, the sliding velocity history at a point on the interface, and the rupture propagation speed. A summary of these experiments and a discussion of the conditions leading to various modes of ruptures is given in the following sections.

#### 4.06.5.1.1 Specimen configuration and loading

Two Homalite-100 plates, subjected to a uniform compressive stress, were frictionally held along the interface. The top plate was also subjected to an asymmetric impact shear loading (Figure 19). Each of the plates was 139.7 mm long, 76.2 mm wide, and 9.525 mm thick. The average roughness of the surfaces in contact was approximately  $R_a = 400 \text{ nm}$ . All

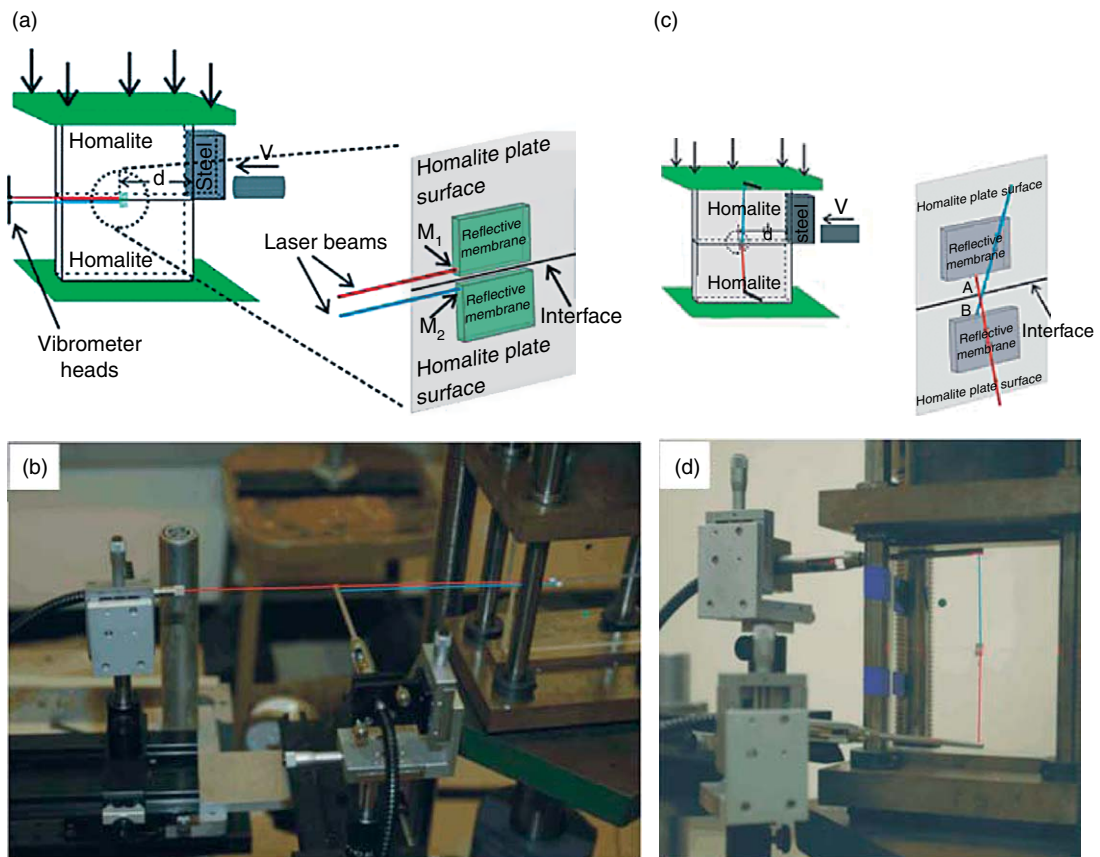


**Figure 19** (a) Schematic illustration of the experimental configuration for the sliding velocity measurement. The area inside the dotted circle is shown magnified. Points  $M_1$  and  $M_2$  were at the same horizontal distance  $d$  from the impact side of the Homalite plate. (b) Photography of the actual setup displaying the arrangement of the velocimeters’ heads for the measurement of the sliding velocity. (c) Schematic illustration of the experimental configuration for the relative vertical velocity measurement. The area inside the dotted line is shown magnified. Points  $M_1$  and  $M_2$  are at the same horizontal distance from the impact side of the Homalite plate. (d) Photography of the actual setup displaying the arrangement of the velocimeters’ heads.

the experiments were executed at the same external confining stress of  $P=10$  MPa, applied by a calibrated press. The asymmetric impact loading was imposed via a cylindrical steel projectile of diameter 25.4 mm and length 50.8 mm, fired using a gas gun. The impact speeds ranged from  $9\text{ m s}^{-1}$  to  $72\text{ m s}^{-1}$ . A steel buffer 73 mm high, 25.4 mm long, and 9.525 mm thick was attached to the impact side of the upper plate to prevent shattering by direct impact and to induce a more or less planar loading wave.

#### 4.06.5.1.2 Using particle velocimetry to measure slip and opening histories

The time evolution of the dynamic stress field in the bulk was recorded by high-speed digital photography in conjunction with dynamic photoelasticity (see Section 4.06.2.1). In addition, a new technique based on laser interferometry was adapted to locally measure the horizontal and vertical components of the in-plane particle velocity at various points above and below the sliding interface, thus allowing for the measurement of slip and opening velocity histories. The combination of the full-field technique of photoelasticity with the local technique of velocimetry is proved to be a very powerful tool in the study of dynamic sliding.

The configuration employed in the measurement of the slip velocity is as follows. A pair of independent fiber-optic velocimeters was used to measure the horizontal particle velocities at two adjacent points  $M_1$  and  $M_2$  across the interface. A schematic illustration of the experimental setup is shown in [Figure 19\(a\)](#), whereas a photograph of the setup is shown in [Figure 19\(b\)](#). The vertical distance of each point from the interface was less than  $250\text{ }\mu\text{m}$ . Both points had the same horizontal distance from the impact side of the Homalite plates. By subtracting the velocity of the point below the interface ( $M_2$ ) from that of the point above the interface ( $M_1$ ), the relative horizontal velocity history was obtained. The velocimeter consists of a modified Mach–Zehnder interferometer and a velocity decoder. The decoder was set to a full range scale of  $\pm 10\text{ m s}^{-1}$  with a maximum frequency of 1.5 MHz and a maximum acceleration of  $10^7\text{ g}$ . The beam spot size was approximately  $70\text{ }\mu\text{m}$ , whereas the error of the velocity measurements was 1%. The technique and the corresponding experimental setup are presented in detail in [Lykotrafitis et al. \(2006b\)](#).

Following the same strategy, a pair of independent velocimeters was employed to measure the vertical in-plane components of the velocities of

two adjacent points  $M_1$  and  $M_2$ , located across the interface. The relative vertical velocity was obtained by adding algebraically the corresponding velocities. The arrangement of the velocimeters is shown schematically in [Figure 19\(c\)](#), whereas a photograph of the actual setup is shown in [Figure 19\(d\)](#). These two types of measurements enabled them to record various modes of rupture propagating along the frictional interface.

#### 4.06.5.2 Visualizing Pulse-Like and Crack-Like Ruptures in the Laboratory

The specimen was subjected to a uniform confining pressure of 10 MPa, whereas the impact speed was  $V=19\text{ m s}^{-1}$ . An instantaneous isochromatic fringe pattern is shown in [Figure 20\(a\)](#). An eye-like fringe structure is observed traveling, from right to left, behind the longitudinal wave front. The rupture tip A followed this fringe structure at a supershear speed of  $1.36C_S$ . Consequently, two Mach lines forming a shear Mach cone emanated from the rupture tip. The tip can be located by tracing the Mach lines to the interface. The rupture-tip speed was found to be constant.

The time evolution of the horizontal relative velocity of two adjacent points  $M_2$  and  $M_1$ , belonging to the upper and lower plate respectively at a horizontal distance of 70 mm from the impact side of the Homalite plate, is displayed in [Figure 20\(b\)](#). If the entire time history of photoelastic frames is taken into consideration in relation to the velocimeter time record, then this record can be superimposed on the photographs (see red line trace in [Figure 20\(a\)](#)) by converting time to spatial distance.

When the longitudinal wave front arrived at the measurement positions  $M_1$  and  $M_2$  of [Figure 20\(a\)](#), where the pair of the interferometers was pointed, the velocities of both points started to increase. However, the relative horizontal velocity was zero for the next few microseconds and it remained very low for a time interval of approximately  $13\text{ }\mu\text{s}$ . A numerical integration of the relative velocity with respect to time from 0 to  $13\text{ }\mu\text{s}$  resulted in an accumulated relative horizontal displacement of  $2\text{ }\mu\text{m}$  between points  $M_1$  and  $M_2$ , which can easily be identified to elastic shear deformation prior to sliding. Indeed, the actual sliding started at approximately  $13\text{ }\mu\text{s}$  when the rupture tip (point A as identified by the photoelastic image) arrived at the measurement position and the relative velocity increased sharply. The correlation between the two

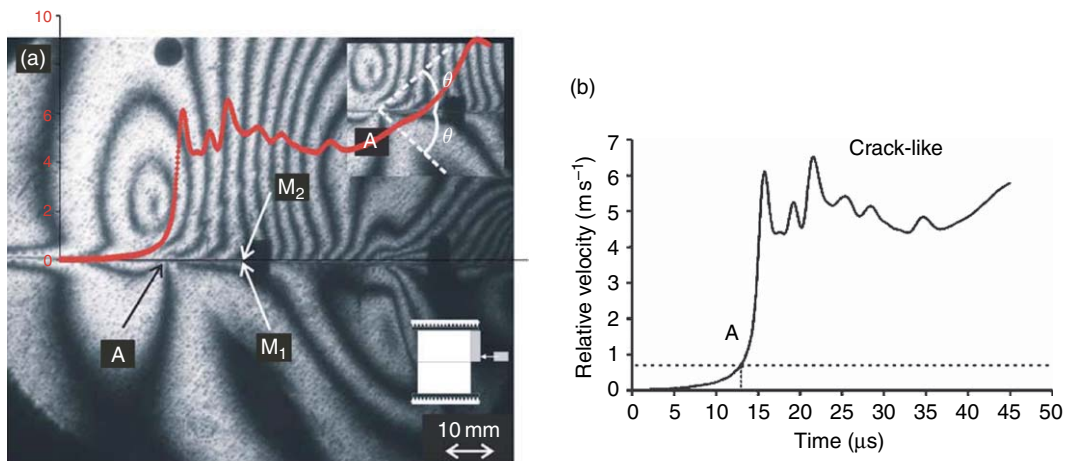


**Figure 20** (a) Isochromatic fringe pattern generated during an experiment for which the impact speed was  $19 \text{ m s}^{-1}$  and the external compression was 10 MPa. The rupture tip is at the fringe concentration point A. The insets highlight the location of the Mach lines emanating from the rupture tip and the specimen configuration. The slip profile is superimposed (red line). (b) Relative velocity history of points  $M_1$  and  $M_2$  located at a distance of 70 mm from the impact side of the Homalite plates. The rupture commenced when the rupture tip A reached the velocity measurement position.

measurements has allowed us to thus establish an estimate of elastic displacement ( $\sim 2 \mu\text{m}$ ) preceding the sliding event for a confining pressure of 10 MPa. After it reached its maximum value of approximately  $6 \text{ m s}^{-1}$ , the relative velocity decreased and then it fluctuated, but never dropped below  $4 \text{ m s}^{-1}$  during the recording time. As is evident from **Figure 20(b)**, the sliding was continuous and thus we can safely say that rupture occurred in a classic crack-like mode.

As was already noted, the speed of the rupture tip was substantially higher than the shear wave speed of Homalite, and therefore the situation is similar to intersonic shear rupture propagation observed to occur along both ‘coherent’ (Rosakis *et al.*, 1999, 2000; Needleman, 1999; Coker and Rosakis, 2001; Samudrala *et al.*, 2002a, 2002b) and ‘incoherent’ (Xia *et al.*, 2004) interfaces separating identical monolithic solids. In the former experiments, the ‘coherent’ interfaces were bonded and they featured intrinsic strength and toughness in the absence of confining pressure. Unlike the present study, the resulting modes were always crack-like and the rupture speeds were not constant throughout the event.

In contrast to these early shear crack growth experiments, the present work involves incoherent or frictional interfaces and static far-field compressive loading. Here, the frictional resistance to sliding depends on the normal stress through the friction law. The normal stress, however, is a superposition of the static externally imposed pressure and a dynamic (inertial) compression generated by the

impact loading as follows. The P-wave produced by the impact loading creates a primarily horizontal compressive stress in the upper plate close to the interface, and due to the Poisson effect it also creates compression in the direction vertical to the interface. As the sliding proceeds, the vertical stress to the rupture interface changes, and thus the friction changes as well. The change in friction, however, affects the evolution of sliding. Thus, we infer that sliding is dependent on impact loading not only through the horizontal compression, which is the driving force for sliding, but also through the vertical compression which affects the resistance to sliding. Because of that dependence, essential changes in the rupture process are to be expected as the impact speed is decreased.

In order to investigate the above line of reasoning, the impact speed was reduced to  $15 \text{ m s}^{-1}$ . **Figure 21(a)** shows an instantaneous isochromatic fringe pattern obtained at the above impact speed. The corresponding relative horizontal velocity history, measured at 30 mm from the impact side of the Homalite plate, is shown in **Figure 21(b)**. By combining the horizontal relative velocity measurement with the recorded photoelastic frames, we can identify two rupture tips  $A_1$  and  $A_2$ , which are fringe concentration points and are propagating along the rupture interface at speeds of  $1.09C_S$  and  $0.98C_S$ , respectively. The deformation at the velocity measurement position remains elastic until approximately  $18 \mu\text{s}$  when the rupture tip  $A_1$  arrived there

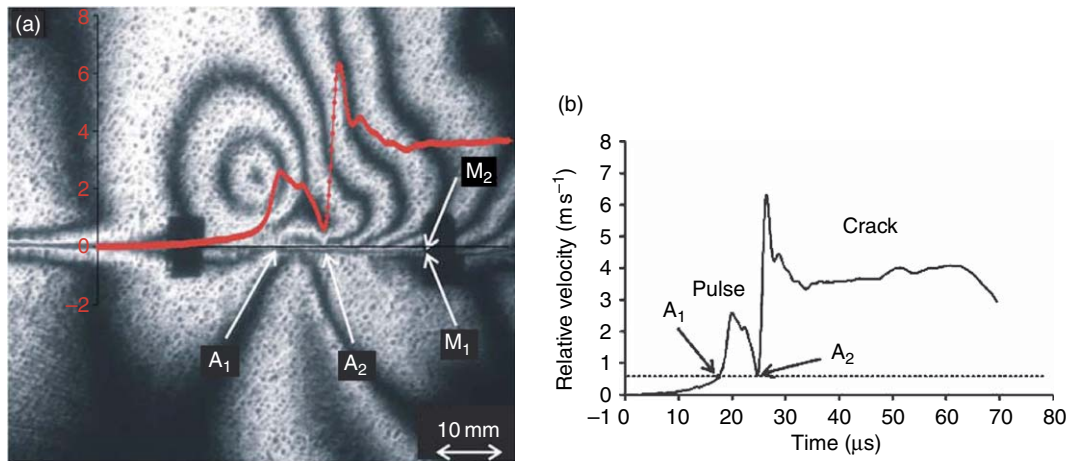


**Figure 21** (a) Isochromatic fringe pattern generated during an experiment for which the impact speed was  $15 \text{ m s}^{-1}$  and the external compression was 10 MPa. The fringe concentration points  $A_1$  and  $A_2$  are the rupture tip and the rear edge respectively of the pulse-like rupture mode. The crack-like mode initiated at  $A_2$  right after the pulse. The slip profile is superimposed (red line). (b) Relative velocity history of points  $M_1$  and  $M_2$  located at a distance of 30 mm from the impact side of the Homalite plates. The rupture commenced when the rupture tip  $A_1$  reached the velocity measurement position and a pulse  $A_1A_2$  was formed. The crack-like rupture mode initiated at  $A_2$  right behind the second pulse.

and sliding commenced. As in the previous case, the commencement of slip corresponds to an accumulated relative horizontal displacement of  $2 \mu\text{m}$ . Subsequently, the horizontal relative velocity increased rapidly from  $0.6 \text{ m s}^{-1}$  to a local maximum of  $2.5 \text{ m s}^{-1}$ . After  $5 \mu\text{s}$ , the relative velocity decreased abruptly back to  $0.6 \text{ m s}^{-1}$  at point  $A_2$  (Figure 21(b)). The slip ceased since the relative velocity was very low, allowing surface asperities to re-establish contact and be deformed elastically. The above observations show that the stable fringe structure ( $A_1A_2$ ) represents a ‘self-healing’ slip pulse of approximately  $7 \mu\text{s}$  in duration. Directly after the pulse, the relative velocity increased rapidly again to  $6.4 \text{ m s}^{-1}$  and retained its large value of approximately  $4 \text{ m s}^{-1}$  for a long period of time, of about  $40 \mu\text{s}$ . This suggests that the initial rupture of the pulse-like mode was immediately followed by a second rupture of the crack-like mode. Thus, as it has been anticipated, the experimental results presented up to this point indicate that the rupture process is very sensitive to impact speed. Indeed, as the projectile speed was decreased while keeping the external confining stress constant, the rupture-tip speed was also decreased. Finally, the rupture mode changed from a crack-like mode to a mixed mode where a single ‘self-healing’ slip pulse was followed by a crack.

By further reducing the impact speed to  $10 \text{ m s}^{-1}$ , the rupture mode became purely pulse-like. The horizontal relative velocity was measured at a

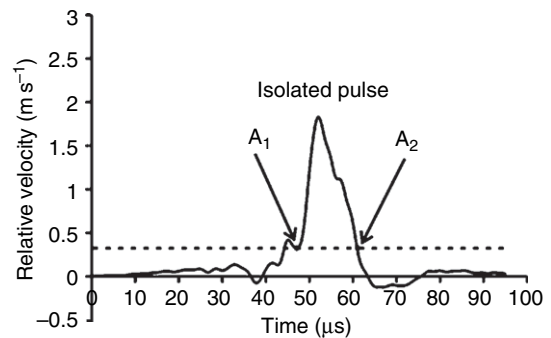


**Figure 22** Relative velocity history of points  $M_1$  and  $M_2$  located at a distance of 70 mm from the impact side of the Homalite plates. The rupture commenced when the rupture tip  $A_1$  reached the velocity measurement position and an isolated pulse  $A_1A_2$  was formed.

distance of 70 mm from the impact side of the Homalite plate and its evolution over time is shown in Figure 22. The rupture started at  $A_1$  and propagated at sub-Rayleigh speed of  $0.76C_S$ , whereas after  $15 \mu\text{s}$  the sliding ceased at  $A_2$ . The duration of sliding was very short compared to the approximately  $100 \mu\text{s}$  duration of the impact event, and thus we infer that an isolated ‘self-healing’ pulse was formed. Such a case clearly indicates that a pulse-like mode of rupture can definitely occur under appropriate conditions. Indeed this is the first time that such a dynamic pulse has been clearly seen in a controlled laboratory setting. The fact that ‘self-healing’ pulses

were obtained as the impact speed was decreased below certain point is consistent with the theoretical results of *Zheng and Rice (1998)*. According to their predictions, and as discussed in Section 4.06.3.1, one of the necessary requirements of self-healing pulse formation is that the overall driving stress could be lower than a threshold value.

The combined use of classic dynamic photoelasticity with velocimetry allowed us to fully characterize the frictional sliding process. However, the maximum particle velocity which can be measured by the velocimeter is  $10 \text{ m s}^{-1}$ . In order to comply with the above limit, low impact speeds were only used up to this point. For higher impact speeds, only dynamic photoelasticity in conjunction with high-speed photography was used as diagnostic tools.

In **Figure 23**, an instantaneous isochromatic fringe pattern is shown at a specific time for the same compressive load of 10 MPa as in the previous experiments and at much higher impact speed of  $42 \text{ m s}^{-1}$ . The rupture propagated intersonically at approximately  $1948 \text{ m s}^{-1} = 1.56 C_S = 0.75 C_P$  giving rise to a shear Mach cone originating from the rupture tip  $B_1$ . In addition, a second Mach line which originated from point  $B_2$  and was nonparallel to the first one was observed behind the rupture point (**Figure 23(a)**). The Mach line was at a shallower slope corresponding to a supershear (approximately sonic) propagation speed of  $2514 \text{ m s}^{-1} = 2.01 C_S = 0.97 C_P$ . A more detailed view of the isochromatic fringe pattern in the neighbor of the rupture tip is shown in the inset of **Figure 23(a)**.

The two shock waves are highlighted by dotted lines. Nonparallel shock lines imply a highly transient and unstable rupture process. Indeed, study of the entire set of the captured photoelastic pictures shows that the tip  $B_1$  of the second Mach line gradually approached the end  $B_2$  of the first Mach line. Finally, these two points merged as the second point caught up with the first point. The sliding continued at the lower speed and thus only one Mach line was observed in the next recorded frames (not shown here). **Figure 23(b)** shows the position histories of the first and second sliding tips for the case above. It is evident that the second sliding tip moved faster than the first sliding tip and at approximately  $50 \mu\text{s}$  the pair of points coalesced. The existence of two Mach lines means that behind the onset of sliding (point  $B_1$ ), there was a second point on the interface (point  $B_2$ ), where the sliding speed again changed rapidly. Then, one could conjecture that the initial sliding which started at point  $B_1$  stopped after a while and new sliding started at point  $B_2$ . In this way, an unstable sliding pulse was formed between the points  $B_1$  and  $B_2$  followed by a crack-like sliding which started at point  $B_2$  in a similar manner to that shown in **Figure 21** though at higher sliding speeds. We finally note that behind the second Mach line a ‘wrinkle’ like pulse appeared at point C propagating at a speed of  $0.92 C_S$  which is close to the Rayleigh wave speed of Homalite. We extensively elaborate on the nature of this disturbance in Section 4.06.5.3.

An important comment on the frictional sliding experiments discussed above is that the rupture-tip

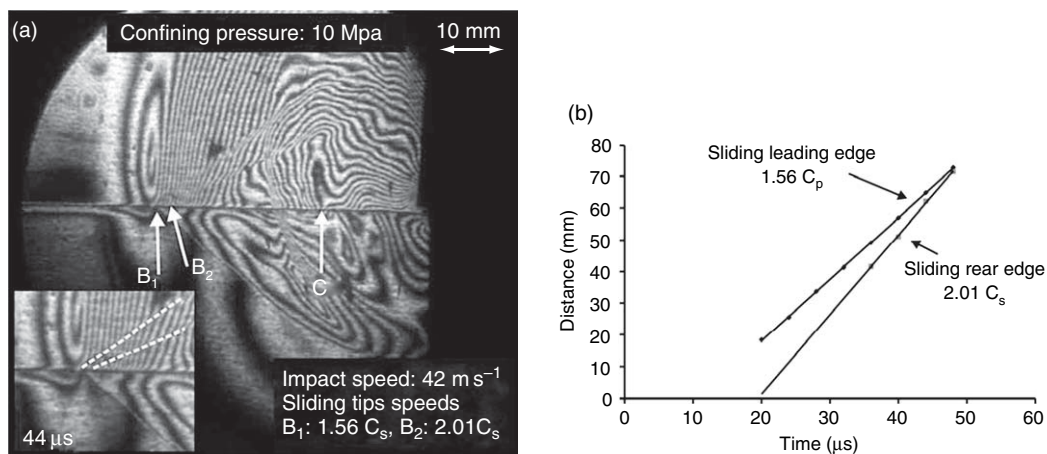


**Figure 23** (a) Isochromatic fringes of sliding propagation at different time instances. Two sliding tips ( $B_1$  and  $B_2$ ) were propagating at different intersonic speeds. In the insets the dual and single Mach lines are marked. (b) Positions of the sliding leading edge and the second sliding tip as functions of time.

speeds were constants during the entire observation time. That is a general result and it holds true for all the experiments performed. This is a strong characteristic of frictional sliding and it agrees with theoretical results (Adams, 1998; Rice *et al.*, 2001; Ranjith and Rice, 2001) which predict constant and discrete propagation speeds for all the different disturbances and singularities along homogeneous interfaces subjected to uniform prestress.

In the last part of this section, the influence of the impact speed on the propagation speeds of the rupture tip is explored. Figure 24 shows the variation of the propagation speed of the sliding front with the impact speed at a constant uniform confining stress of 10 MPa. The slowest achieved impact speed was  $9 \text{ m s}^{-1}$ . In this case and in other cases with impact speeds close to  $10 \text{ m s}^{-1}$  the rupture-tip speed was sub-Rayleigh. At higher impact speeds the rupture-tip speed became supershear. It was observed that for impact speeds in the range of 20 to  $40 \text{ m s}^{-1}$ , the sliding speed was slightly above  $\sqrt{2}C_S$ . This is a special rupture speed (also discussed in Sections 4.06.3.1, 4.06.4.3, and 4.06.4.5) and it has been shown that it separates regions of unstable and stable inter-sonic shear crack growth (Samudrala *et al.*, 2002a, 2002b). When the impact speed increased, the rupture-tip speed increased toward the plane stress P-wave speed. It is worth mentioning that no sliding speed was observed in the interval between the Rayleigh wave speed and the shear wave speed of Homalite-100. This experimental observation agrees with theoretical predictions on steady-state shear crack propagation which exclude this speed interval based on energetic arguments (Freund, 1990; Broberg, 1999; Rosakis, 2002). It should also be noted that the experimental rupture-tip speed measurements presented here feature, as is proven below,

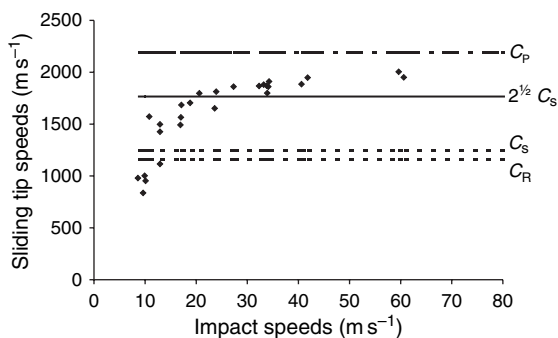


**Figure 24** Variation of the sliding tip speed with the impact speed. The confining stress was 10 MPa.

high-enough resolution to obtain propagation speeds in the interval between  $C_R$  and  $C_S$ , if such speeds existed. It is finally noted that experiments performed at lower compression show that the speed of the rupture tip was influenced by the change in the static confining stress and it was supershear even at the lowest achieved impact speed.

#### 4.06.5.3 Wrinkle-Like Opening Pulses along Interfaces in Homogeneous Systems

The possibility of generating wrinkle-like sliding pulses in incoherent frictionless contact between two dissimilar solids, when separation does not occur, was first investigated by Achenbach and Epstein (1967). These ‘smooth contact Stonely waves’ (also known as slip waves or generalized Rayleigh waves) are qualitatively similar to those of bonded contact (Stonely waves) and occur for a wider range of material combinations. Comninou and Dundurs (1977) found that self-sustained slip waves with interface separation (detachment waves or wrinkle-like opening slip pulses) can propagate along the interface of two similar or dissimilar solids which are pressed together. The constant propagation speed of these waves was found to be between the Rayleigh wave speed and the shear wave speed of the slowest wave speed material. For interfaces separating identical solids the propagation speed was between  $C_R$  and  $C_S$ . Weertman (1980) obtained a 2-D self-sustained wrinkle-like slip pulse propagating at the generalized Rayleigh wave speed along a bimaterial interface governed by Coulomb friction when the remote shear stress was less than the frictional strength of the interface. Finite-difference calculations of Andrews and Ben-Zion (1997) show the propagation of wrinkle-like opening pulses along a bimaterial interface governed by Coulomb friction. Particle displacement in a direction perpendicular to the fault is much greater in the slower material than in the faster material, resulting in a separation of the interface during the passage of the slip pulse. Anooshehpour and Brune (1999) discovered such waves in rubber sliding experiments (using a bimaterial system consisting of two rubber blocks with different wave speeds). The above-mentioned detachment waves are radically different from the Schallamach waves (Schallamach, 1971) which propagate very slowly compared to the wave speeds of the solid.

Lykotrafitis and Rosakis (2006b) observed wrinkle-like opening pulses propagating along the interfaces of Homalite-steel bimaterial structures

subjected to impact shear loading. The propagation speeds of these wrinkle-like pulses of finite opening were constants and their values were always between the Rayleigh wave speed and the shear wave speed of Homalite, in accordance with the theoretical prediction of *Comninou and Dundurs (1977)*. The wrinkle-like pulse in the bimaterial case generated a characteristic fringe pattern. Similar photoelastic fringe structures propagating behind the rupture tip along interfaces in homogeneous systems of Homalite were also observed by the same researchers (*Lykotrafitis and Rosakis, 2006a*). Prompted by this similarity, they decided to investigate whether wrinkle-like pulses were once more responsible for the generation of these fringe structures, in interfaces separating identical solids. Their results are summarized in this section. It is known that a system consisting of two identical half-planes and subjected to compression and to far-field shear loading cannot sustain a wrinkle-like pulse propagating along the interface. In the setup used in these experiments, however, the loading was not strictly shear and there is not any physical reason to exclude the possibility of generating wrinkle-like pulses.

In this section, photoelasticity and velocimetry is used to investigate the physical attainability of such wrinkle-like pulses along frictional interfaces separating identical solids. The equivalent issue for the case of Homalite-steel bimaterial system was investigated by *Lykotrafitis and Rosakis (2006b)* and *Lykotrafitis et al. (2006b)*. **Figure 25** is used to illustrate the

methodology used to identify the wrinkle pulses. The figure features an instantaneous isochromatic fringe pattern obtained at confining stress of 10 MPa and at an impact speed of  $28 \text{ m s}^{-1}$ . Point B is of particular interest. The rupture tip A is shown to propagate at a constant supershear speed of  $1.49 C_S$ . A shear Mach cone is clearly visible in the photoelastic image. A fringe structure located at point B, in **Figure 25(a)**, propagates at a speed of  $0.96 C_S$ . The time evolution of the relative vertical displacement of points  $M_1$  and  $M_2$ , which were located 70 mm from the impact side of the Homalite plate, is displayed in **Figure 25(b)**. A simple 1-D calculation shows that the initial static compression of 10 MPa caused a negative relative displacement of approximately  $1.3 \mu\text{m}$ . Negative relative displacement means that the two points approached each other under compression. The P-wave front arrives at about  $2.5 \mu\text{s}$  after the triggering of the oscilloscope. Because of the Poisson effect, the horizontal dynamic (inertial) compression generated a vertical dynamic compression in addition to the static compression. A negative relative displacement was caused by this dynamic compression. The shear rupture point crossed the velocity measurement position at approximately  $10 \mu\text{s}$  (marked A in **Figure 25(b)**) and it did not cause any visible change to the vertical components of the velocities of points  $M_1$  and  $M_2$ . The relative vertical displacement becomes positive at approximately  $31 \mu\text{s}$ . The photoelastic picture, captured at  $30 \mu\text{s}$ , clearly shows that the fringe structure at B, which is the point under

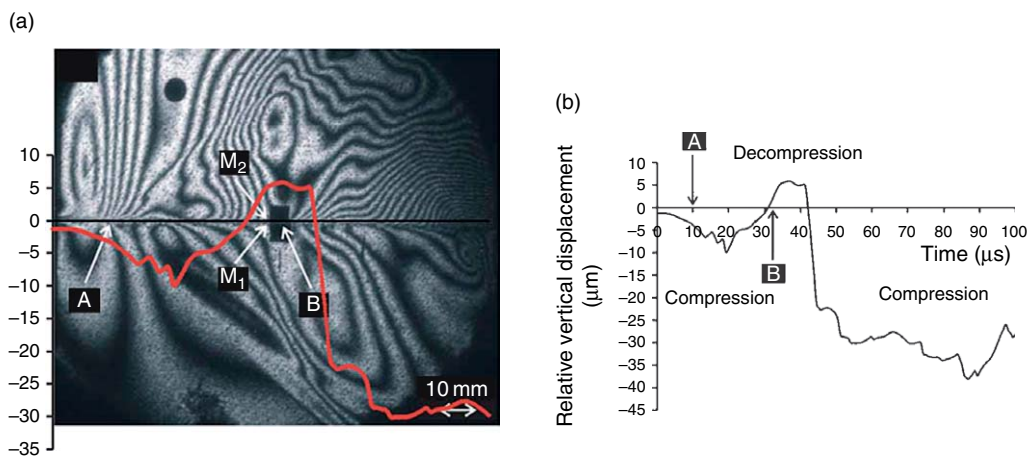


**Figure 25** (a) Isochromatic fringe pattern generated during an experiment for which the impact speed was  $28 \text{ m s}^{-1}$  and the external compression was 10 MPa. The rupture tip is at the fringe concentration point A and the wrinkle-like pulse is at point B. The relative vertical displacement profile is superimposed (red line). (b) Relative vertical displacement history of points  $M_1$  and  $M_2$ , located at a distance of 70 mm from the impact side of the Homalite plate. The rupture tip and the wrinkle-like disturbance crossed the velocity measurement position at approximately  $10 \mu\text{s}$  and  $32 \mu\text{s}$  after triggering, respectively.

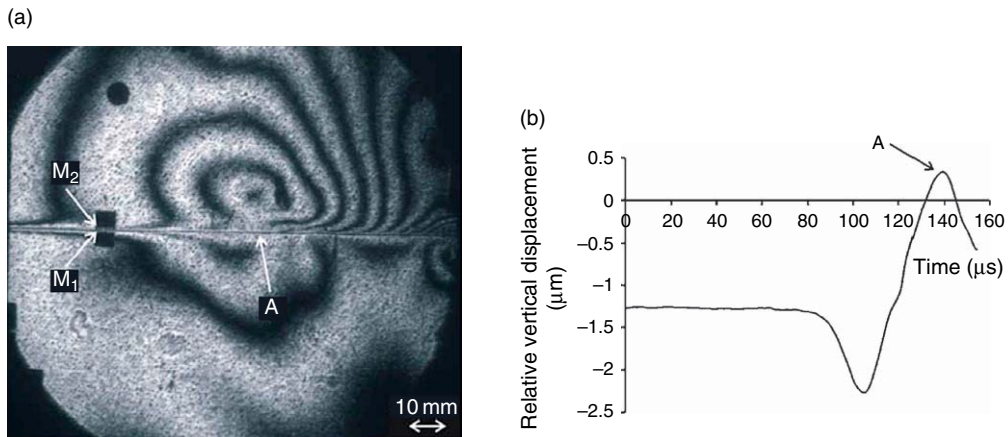


**Figure 26** (a) Isochromatic fringe pattern generated during an experiment for which the impact speed was  $9 \text{ m s}^{-1}$  and the external compression was 10 MPa. The rupture tip is at the fringe concentration point A. No wrinkle-like pulse appeared. (b) Relative vertical displacement history of points  $M_1$  and  $M_2$  located at a distance of 100 mm from the impact side of the Homalite plate.

investigation, is very close to the measurement position. The study of the entire set of the 16 recorded photoelastic images in combination with the relative vertical displacement history sheds light on the distribution of the dynamic compression along the interface during sliding. The interface was locally under dynamic compression immediately after the arrival of the P-wave front until the arrival of the mentioned fringe formation at B. The entire area from the rupture point A to the location of the fringe structure at B was sliding under compression. The length of the area AB was estimated to be approximately 40 mm, whereas the entire length of the interface was 139.7 mm. The fringe structure at B caused a local opening ( $\sim 5 \mu\text{m}$ ) at the interface. At approximately  $42 \mu\text{s}$  the relative vertical displacement became again negative and the compression increased abruptly. During the rest of the recording time the interface at the velocity measurement position was sliding under compression. The fringe structure at B can thus be clearly related to a wrinkle-like pulse propagating along the interface. As was stated earlier, its propagation speed was very close to  $0.96 C_S$  which lies in the interval between the shear and the Rayleigh wave speeds of the material in agreement with the prediction of Comninou and Dundurs (1977).

Reviewing the results from the entire spectrum of experiments, it is verified that, at a confining stress of 10 MPa, the lowest impact speed which can generate a wrinkle-like pulse in the present setup is approximately  $17 \text{ m s}^{-1}$ . Figure 26(a) displays an isochromatic fringe pattern obtained at a confining stress of 10 MPa and at an impact speed of  $9 \text{ m s}^{-1}$ . It

is clear that no fringe structure related to a wrinkle-like pulse appears. That is reflected by the relative vertical displacement history shown in Figure 26(b), where the maximum positive value of the displacement was only about  $0.3 \mu\text{m}$ . A comparison of the photoelastic image shown in Figure 26(a) with photoelastic images obtained at the same static compression of 10 MPa and at similar impact speeds during experiments where the horizontal particle velocities measurements were available, shows that the rupture started at point A.

The propagation speeds of wrinkle-like pulses at different impact speeds and at the same confining stress of 10 MPa are shown in Figure 27. The sliding speed was measured to be between the Rayleigh wave and the shear wave speed of Homalite-100. This result, in combination with the experimental results obtained via velocimetry, favors our conjecture that the interface disturbance was actually a wrinkle-like pulse. As has been already mentioned, the available theoretical and numerical analysis on the subject predicts the same speed range with this identified in Figure 27. It is also noted that both the prestress and the impact speed do not affect the propagation speed of the wrinkle-like pulses provided that such pulses could be generated.

#### 4.06.5.4 Discussion

Finite element calculations of dynamic frictional sliding between deformable bodies have always been a very challenging task for the numerical analysts. As it was recently recognized (see Section

4.06.4.1), the main source of difficulty was the ill-posedness of the corresponding boundary and initial value problem, if a rich-enough friction law was not implemented. Coker *et al.* (2005) took advantage of the latest advances in the theory of the frictional sliding (Rice, 2001) and by using a rate-enhanced, rate and state friction law of Prakash–Clifton type, they were able to perform stable (grid-size independent) finite element calculations for a configuration very similar to the experiments described above. The use of a rate-enhanced Prakash–Clifton type of law was an essential element for the successful completion of the simulations because of the presence of fast changes of the local compression at the interface, caused by wave propagation, during dynamic sliding. As it is explained in Section 4.06.4.1, the Prakash–Clifton law is currently considered the only friction law which correctly describes the effect of fast changes in compression on the resulting frictional

resistance. We note that for various impact speeds the numerical simulations exhibit a richer behavior than the experimental results and generate not only crack-like, pulse-like and mixed mode ruptures but also trains of pulses and pulses following a crack-like rupture. A representative result is shown in Figure 28(a), where the distributions of the sliding speed ( $\Delta\dot{u}_{\text{slip}}$ ) and the shear traction  $T_s$  along the interface at three times ( $t=32, 38, 44 \mu\text{s}$ ) are illustrated, for the case of 40 MPa static compression and of a  $2 \text{ m s}^{-1}$  impact speed. Contours of maximum shear stress, which correspond to isochromatic fringes in photoelasticity, at  $t=38 \mu\text{s}$  are shown in Figure 28(b). In this numerical experiment, a mixed mode of rupture, where a pulse was followed by a crack-like rupture, was obtained. This is reminiscent of the experimental case shown in Figure 21. We believe that the similarity between the numerical and the experimental results can be further improved by binding and eventually fine tuning the parameters of the friction law.

The experimental results presented in Section 4.06.5 elucidate the sliding process and provide conclusive evidence of the occurrence of various sliding rupture modes (crack-like, pulse-like, or mixed) propagating dynamically along incoherent interfaces. Of particular interest here is the experimental evidence of the formation of both supershear and sub-Rayleigh sliding pulses of the ‘self-healing’ type, leading the direct validation of predictions made on the basis of theoretical and numerical models of dynamic shear rupture. These pulses were found to propagate in the absence of interfacial opening. The experiments also provide hints of the dominant physical mechanisms

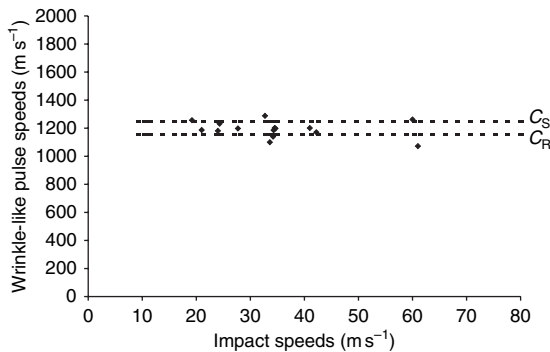


**Figure 27** The wrinkle-like pulse speed remained between the Rayleigh wave speed and the shear wave speed of Homalite-100, independent of the impact speed.

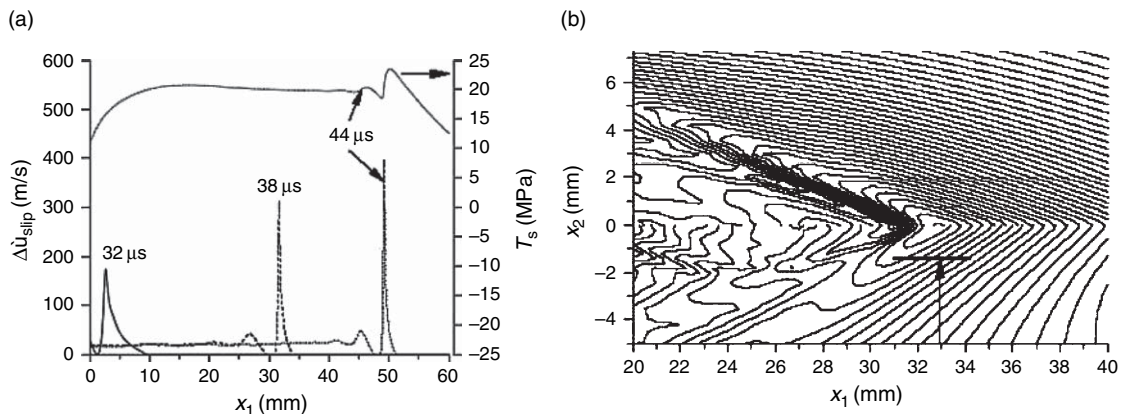


**Figure 28** (a) Distributions of the sliding speed ( $\Delta\dot{u}_{\text{slip}}$ ) at  $t=32, 38,$  and  $44 \mu\text{s}$ , and of the shear traction ( $T_s$ ) at  $t=44 \mu\text{s}$  along the interface for external compression of 40 MPa and impact speed of  $2 \text{ m s}^{-1}$ . (b) Contours of maximum shear stress (isochromatic fringe pattern) at  $t=38 \mu\text{s}$ .

governing the choice of various rupture modes and their evolution. It is finally noted that ‘wrinkle-like’ pulses which feature finite opening in addition to sliding were discovered propagating along the interface at speeds between  $C_R$  and  $C_S$  for various loading conditions.

## Acknowledgments

The authors gratefully acknowledge the support of NSF (Grant EAR 0207873), the US Department of Energy (Grant DE-FG52-06NA 26209) and the consistent support of the Office of Naval Research through (Grant N00014-03-1-0435) and MURI (Grant N000140610730) Dr. Y.D.S. Rajapakse, Program Manager.

## References

- Aagaard BT and Heaton TH (2004) Near-source ground motions from simulations of sustained intersonic and supersonic fault ruptures. *Bulletin of the Seismological Society of America* 94: 2064–2078.
- Aagaard BT, Heaton TH, and Hall JF (2001) Dynamic earthquake ruptures in the presence of lithostatic normal stresses: Implications for friction models and heat production. *Bulletin of the Seismological Society of America* 91: 1765–1796.
- Achenbach JD and Epstein HI (1967) Dynamic interaction of a layer and a half-space. *Journal of Engineering Mechanics* 5: 27–42.
- Abraham FF and Gao HJ (2000) How fast can cracks propagate? *Physical Review Letters* 84: 3113–3116.
- Adams GG (1995) Self-excited oscillations of two elastic half-spaces sliding with a constant coefficient of friction. *Journal of Applied Mechanics-Transactions of the ASME* 62(4): 867–872.
- Adams GG (1998) Steady sliding of two elastic half-spaces with friction reduction due to interface stick-slip. *Journal of Applied Mechanics-Transactions of the ASME* 65(2): 470–475.
- Adams GG (2001) An intersonic slip pulse at a frictional interface between dissimilar materials. *Journal of Applied Mechanics-Transactions of the ASME* 68(1): 81–86.
- Aki K (1979) Characterization of barriers on an earthquake fault. *Journal of Geophysical Research* 84(6): 140–48.
- Andrews DJ (1976) Rupture velocity of plane strain shear cracks. *Journal of Geophysical Research* 81(32): 5679–5687.
- Andrews DJ (1985) Dynamic plane-strain shear rupture with a slip-weakening friction law calculated by a boundary integral method. *Bulletin of the Seismological Society of America* 75(1): 1–21.
- Andrews DJ and Ben-Zion Y (1997) Wrinkle-like slip pulse on a fault between different materials. *Journal of Geophysical Research-Solid Earth* 102(B1): 553–571.
- Andrews DJ and Harris RA (2005) The wrinkle-like slip pulse is not important in earthquake dynamics. *Geophysical Research Letters* 32(23): L23303 doi: 10.1029/2005GL023996.
- Anooshehpour A and Brune JN (1994) Frictional heat-generation and seismic radiation in a foam rubber model of earthquakes. *Pure and Applied Geophysics* 142(3–4): 735–747.
- Anooshehpour A and Brune JN (1999) Wrinkle-like Weertman pulse at the interface between two blocks of foam rubber with different velocities. *Geophysical Research Letters* 26(13): 2025–2028.
- Archuleta RJ (1984) A faulting model for the 1979 Imperial-Valley Earthquake. *Journal of Geophysical Research* 89(NB6): 4559–4585.
- Beeler NM and Tullis TE (1996) Self-healing slip pulses in dynamic rupture models due to velocity-dependent strength. *Bulletin of the Seismological Society of America* 86: 1130–1148.
- Ben-Zion Y (2001) Dynamic ruptures in recent models of earthquake faults. *Journal of the Mechanics and Physics of Solids* 49(9): 2209–2244.
- Ben-Zion Y (2006) Comment on “Material contrast does not predict earthquake rupture propagation direction” by R. A. Harris and S. M. Day. *Geophysical Research Letters* 33(13): L13310 doi: 10.1029/2005GL025652.
- Ben-Zion Y and Huang YQ (2002) Dynamic rupture on an interface between a compliant fault zone layer and a stiffer surrounding solid. *Journal of Geophysical Research-Solid Earth* 107(B2): 2042 doi: 10.1029/2001JB000254.
- Ben-Zion Y and Rice JR (1997) Dynamic simulations of slip on a smooth fault in an elastic solid. *Journal of Geophysical Research-Solid Earth* 102(B8): 17771–17784.
- Bouchon M, Bouin MP, Karabulut H, Toksoz MN, Dietrich M, and Rosakis AJ (2001) How fast is rupture during an earthquake? New insights from the 1999 Turkey earthquakes. *Geophysical Research Letters* 28(14): 2723–2726.
- Bouchon M and Vallee M (2003) Observation of long supershear rupture during the magnitude 8.1 Kunlunshan earthquake. *Science* 301(5634): 824–826.
- Bowden FP and Tabor D (1986) *The friction and lubrication of solids*, 374 pp. Oxford: Clarendon Press.
- Brace WF and Byerlee JD (1966) Stick-slip as a mechanism for earthquakes. *Science* 153(3739): 990–992.
- Broberg KB (1999) *Cracks and fracture*, 725 pp. San Diego: Academic Press.
- Brune JN (1973) Earthquake modeling by stick-slip along pre-cut surfaces in stressed from rubber. *Bulletin of the Seismological Society of America* 63(6): 2105–2119.
- Brune JN (1976) The physics of earthquake strong motion. In: Lomnitz C and Rosenbluth E (eds.) *Seismic Risk and Engineering Decisions*, pp. 141–171. New York: Elsevier.
- Brune JN and Anooshehpour A (1997) Frictional resistance of a fault zone with strong rotors. *Geophysical Research Letters* 24(16): 2071–2074.
- Brune JN, Brown S, and Johnson PA (1993) Rupture mechanism and interface separation in foam rubber models of earthquakes - A possible solution to the heat-flow paradox and the paradox of large overthrusts. *Tectonophysics* 218(1–3): 59–67.
- Burridge R (1973) Admissible speeds for plane-strain self-similar shear cracks with friction but lacking cohesion. *Geophysical Journal of the Royal Astronomical Society* 35(4): 439–455.
- Burridge R, Conn G, and Freund LB (1979) Stability of a rapid mode-I shear crack with finite cohesive traction. *Journal of Geophysical Research* 84(NB5): 2210–2222.
- Cochard A and Madariaga R (1994) Dynamic faulting under rate-dependent friction. *Pure and Applied Geophysics* 142(3–4): 419–445.
- Cochard A and Madariaga R (1996) Complexity of seismicity due to highly rate-dependent friction. *Journal of Geophysical Research* 105: 25891–25907.
- Cochard A and Rice JR (2000) Fault rupture between dissimilar materials: Ill-posedness, regularization, and slip-pulse response. *Journal of Geophysical Research-Solid Earth* 105(B11): 25891–25907.

- Coker D, Lykotraftitis G, Needleman A, and Rosakis AJ (2005) Frictional sliding modes along an interface between identical elastic plates subject to shear impact loading. *Journal of the Mechanics and Physics of Solids* 53: 884–922.
- Coker D and Rosakis AJ (2001) Experimental observations of intersonic crack growth in asymmetrically loaded unidirectional composite plates. *Philosophical Magazine A-Physics of Condensed Matter Structure Defects and Mechanical Properties* 81(3): 571–595.
- Coker D, Rosakis AJ, and Needleman A (2003) Dynamic crack growth along a polymer composite-Homalite interface. *Journal of the Mechanics and Physics of Solids* 51(3): 425–460.
- Comninou M and Dundurs J (1977) Elastic interface waves involving separation. *Journal of Applied Mechanics-Transactions of the ASME* 44(2): 222–226.
- Dally JW and Riley WF (1991) *Experimental Stress Analysis*, 639 pp. New York: McGraw-Hill.
- Das S and Aki K (1977) Numerical study of 2-dimensional spontaneous rupture propagation. *Geophysical Journal of the Royal Astronomical Society* 50(3): 643–668.
- Day SM (1982) 3-dimensional simulation of spontaneous rupture - The effect of nonuniform prestress. *Bulletin of the Seismological Society of America* 72(6): 1881–1902.
- Dieterich JH (1972) Time-dependent friction in rocks. *Journal of Geophysical Research* 77(20): 3690–3697.
- Dieterich JH (1979) Modeling of rock friction. 1. Experimental results and constitutive equations. *Journal of Geophysical Research* 84(NB5): 2161–2168.
- Dieterich JH (1992) Earthquake nucleation on faults with rate-dependent and state-dependent strength. *Tectonophysics* 211(1–4): 115–134.
- Dieterich JH and Kilgore BD (1994) Direct observation of frictional contacts - New insights for state-dependent properties. *Pure and Applied Geophysics* 143(1–3): 283–302.
- Di Toro G, Goldsby DL, and Tullis TE (2004) Friction falls toward zero in quartz rock as slip velocity approaching seismic rates. *Nature* 427: 436–439.
- Dunham EM, Favreau P, and Carlson JM (2003) A supershear transition mechanism for cracks. *Science* 299(5612): 1557–1559.
- Eberhart-Phillips D and Michael AJ (1998) Seismotectonics of the Loma Prieta, California, region determined from three-dimensional V-p, V-p/V-s, and seismicity. *Journal of Geophysical Research-Solid Earth* 103(B9): 21099–21120.
- Ellsworth WL, Çelebi M, Evans JR, Jensen EG, Nyman DJ, and Spudich P (2004) Processing and Modeling of the Pump Station 10 Record from the November 3, 2002, Denali Fault, Alaska Earthquake. In: *Proceedings of the Eleventh International Conference of Soil Dynamics and Earthquake Engineering*. Berkeley, CA, pp. 563 Jan. 7–9.
- Freund LB (1990) *Dynamic Fracture Mechanics*. Cambridge: Cambridge University Press.
- Fukuyama E and Madariaga R (1998) Rupture dynamics of a planar fault in a 3D elastic medium: Rate- and slip-weakening friction. *Bulletin of the Seismological Society of America* 88(1): 1–17.
- Gao HJ, Huang YG, and Abraham FF (2001) Continuum and atomistic studies of intersonic crack propagation. *Journal of the Mechanics and Physics of Solids* 49(9): 2113–2132.
- Geubelle PH and Kubair DV (2001) Inter-sonic crack propagation in homogeneous media under shear-dominated loading: Numerical analysis. *Journal of the Mechanics and Physics of Solids* 49(3): 571–587.
- Gu YJ and Wong TF (1994) Development of shear localization in simulated quartz gouge - Effect of cumulative slip and gouge particle-size. *Pure and Applied Geophysics* 143(1–3): 387–423.
- Harris RA and Day SM (1993) Dynamics of fault interaction - Parallel strike-slip faults. *Journal of Geophysical Research-Solid Earth* 98(B3): 4461–4472.
- Harris RA and Day SM (1997) Effects of a low-velocity zone on a dynamic rupture. *Bulletin of the Seismological Society of America* 87(5): 1267–1280.
- Harris RA and Day SM (2005) Material contrast does not predict earthquake rupture propagation direction. *Geophysical Research Letters* 32(23): L23301 doi:10.1029/2005GL023941.
- Hartzell SH and Heaton TH (1983) Inversion of strong ground motion and teleseismic waveform data for the fault rupture history of the 1979 Imperial Valley, California, earthquake. *Bulletin of the Seismological Society of America* 73: 1553–1583.
- Heaton TH (1982) The 1971 San Fernando earthquake; a double event?. *Bulletin of the Seismological Society of America* 72: 2037–2062.
- Heaton TH (1990) Evidence for and implications of self-healing pulses of slip in earthquake rupture. *Physics of the Earth and Planetary Interiors* 64(1): 1–20.
- Ibrahim RA (1994) Friction-induced vibration, chatter, squeal, and chaos, Part I: Mechanics of contact and friction. *Applied Mechanics Review ASME* 47: 209–226.
- Ida Y (1972) Cohesive force across tip of a longitudinal-shear crack and Griffiths specific surface-energy. *Journal of Geophysical Research* 77(20): 3796–3805.
- Ide S and Takeo M (1997) Determination of constitutive relations of fault slip based on seismic wave analysis. *Journal of Geophysical Research-Solid Earth* 102(B12): 27379–27391.
- Johnson E (1990) On the initiation of unidirectional slip. *Geophysical Journal International* 101: 125–132.
- Johnson TL and Scholz CH (1976) Dynamic properties of stick-slip friction of rock. *Journal of Geophysical Research* 81(5): 881–888.
- Kanamori H (1994) Mechanics of earthquakes. *Annual Review of Earth and Planetary Sciences* 22: 207–237.
- Kubair DV, Geubelle PH, and Huang YGY (2003) Analysis of a rate-dependent cohesive model for dynamic crack propagation. *Engineering Fracture Mechanics* 70(5): 685–704.
- Kubair DV, Geubelle PH, and Huang YY (2002) Inter-sonic crack propagation in homogeneous media under shear-dominated loading: theoretical analysis. *Journal of the Mechanics and Physics of Solids* 50(8): 1547–1564.
- Lambros J and Rosakis AJ (1995) Dynamic decohesion of bimaterials - experimental-observations and failure criteria. *International Journal of Solids and Structures* 32(17–18): 2677–2702.
- Lapusta N, Rice JR, Ben-Zion Y, and Zheng G (2000) Elastodynamic analysis for slow tectonic loading with spontaneous rupture episodes on faults with rate- and state-dependent friction. *Journal of Geophysical Research* 105: 23,765–23,789.
- Lapusta N and Rice JR (2003) Nucleation and early seismic propagation of small and large events in a crustal earthquake model. *Journal of Geophysical Research-Solid Earth* 108(B4): 2205 (doi:10.1029/2001JB000793).
- Le Pichon X, Chamot-Rooke N, Rangin C, and Sengor AMC (2003) The North Anatolian fault in the Sea of Marmara. *Journal of Geophysical Research-Solid Earth* 108(B4) 2170–2179.
- Lin AM, Fu BH, Guo JM, et al. (2002) Co-seismic strike-slip and rupture length produced by the 2001 M-s 8.1 Central Kunlun earthquake. *Science* 296(5575): 2015–2017.
- Liu HL and Helmberger DV (1983) The near-source ground motion of the 6 August 1979 Coyote Lake, California, earthquake. *Bulletin of the Seismological Society of America* 73: 201–218.

- Lu X, Lapusta N, and Rosakis AJ (2005) Testing friction laws by comparing simulation results with experiments of spontaneous dynamic rupture. *EOS Transactions of the American Geophysical Union Fall Meet. Suppl.*, Abstract S32B-07.
- Lykotrafitis G and Rosakis AJ (2006a) Sliding along frictionally held incoherent interfaces in homogeneous systems subjected to dynamic shear loading: A photoelastic study. *International Journal of Fracture* 140: 213–233.
- Lykotrafitis G and Rosakis AJ (2006b) Dynamic sliding of frictionally held bimaterial interfaces subjected to impact shear loading. *Proceedings of the Royal Society of London, Series A* 462: 2997–3026.
- Lykotrafitis G, Rosakis AJ and Ravichandran G (2006a) Self-healing pulse-like shear ruptures in the laboratory. *Science* 313: 1765–1768.
- Lykotrafitis G, Rosakis AJ, and Ravichandran G (2006b) Particle velocimetry and photoelasticity applied to the study of dynamic sliding along frictionally-held bimaterial interfaces: Techniques and feasibility. *Experimental Mechanics* 46: 205–216.
- Madariaga R (1976) Dynamics of an expanding circular fault. *Bulletin of the Seismological Society of America* 66: 639–666.
- Madariaga R and Olsen KB (2000) Criticality of rupture dynamics in 3-D. *Pure and Applied Geophysics* 157(11–12): 1981–2001.
- Magistrale H and Sanders C (1995) P-wave image of the peninsular ranges Batholith, Southern California. *Geophysical Research Letters* 22(18): 2549–2552.
- Mendoza C and Hartzell SH (1988) Inversion for slip distribution using GDSN P waves: North Palm Springs, Borah peak, and Michoacan earthquakes. *Bulletin of the Seismological Society of America* 78: 1092–1111.
- Mendoza C and Hartzell SH (1989) Slip distribution of 19 September 1985 Michoacan, Mexico, earthquake: Near-source and teleseismic constraints. *Bulletin of the Seismological Society of America* 79: 655–669.
- McGuire JJ, Zhao L, and Jordan TH (2002) Predominance of unilateral rupture for a global catalog of large earthquakes. *Bulletin of the Seismological Society of America* 92(8): 3309–3317.
- Needleman A (1999) An analysis of intersonic crack growth under shear loading. *ASME, Journal of Applied Mechanics* 66: 847–857.
- Nielsen S and Madariaga R (2003) On the self-healing fracture mode. *Bulletin of the Seismological Society of America* 93: 2375–2388.
- Nielsen SB, Carlson JM, and Olsen KB (2000) Influence of friction and fault geometry on earthquake rupture. *Journal of Geophysical Research-Solid Earth* 105(B3): 6069–6088.
- Ohnaka M (2003) A constitutive scaling law and a unified comprehension for frictional slip failure, shear fracture of intact rock, and earthquake rupture. *Journal of Geophysical Research-Solid Earth* 108(B2): 2080 doi:10.1029/2000JB000123.
- Ohnaka M and Shen LF (1999) Scaling of the shear rupture process from nucleation to dynamic propagation: Implications of geometric irregularity of the rupturing surfaces. *Journal of Geophysical Research-Solid Earth* 104(B1): 817–844.
- Okubo PG and Dieterich JH (1984) Effects of Physical Fault Properties on Frictional Instabilities Produced on Simulated Faults. *Journal of Geophysical Research* 89(NB7): 5817–5827.
- Olsen KB, Madariaga R, and Archuleta RJ (1997) Three-dimensional dynamic simulation of the 1992 Landers earthquake. *Science* 278(5339): 834–838.
- Palmer AC and Rice JR (1973) Growth of slip surfaces in progressive failure of over-consolidated clay. *Proceedings of the Royal Society of London Series A-Mathematical Physical and Engineering Sciences* 332(1591): 527–548.
- Papageorgiou A and Aki K (1983a) A specific barrier model for the quantitative description of inhomogeneous faulting and the prediction of strong ground motion. I. Description of the model. *Bulletin of the Seismological Society of America* 73: 693–722.
- Papageorgiou A and Aki K (1983b) A specific barrier model for the quantitative description of inhomogeneous faulting and the prediction of strong ground motion. II. Applications of the model. *Bulletin of the Seismological Society of America* 73: 953–978.
- Parsons T, Toda S, Stein RS, Barka A, and Dieterich JH (2000) Heightened odds of large earthquakes near Istanbul: An interaction-based probability calculation. *Science* 288(5466): 661–665.
- Pelton JR, Meissner CW, and Smith KD (1984) Eyewitness account of normal surface faulting. *Bulletin of the Seismological Society of America* 74: 1083–1089.
- Peltzer G, Crampe F, and King G (1999) Evidence of nonlinear elasticity of the crust from the Mw7.6 Manyi (Tibet) earthquake. *Science* 286(5438): 272–276.
- Perrin G, Rice JR, and Zheng G (1995) Self-healing slip pulse on a frictional surface. *Journal of the Mechanics and Physics of Solids* 43: 1461–1495.
- Prakash V and Clifton RJ (1993) Time resolved dynamic friction measurements in pressure-shear. In: Ramesh KT (ed.) *Experimental Techniques in the Dynamics of Deformable Solids* Applied mechanics division, pp. 33–48. New York: ASME.
- Prakash V (1998) Frictional response of sliding interfaces subjected to time varying normal pressures. *Journal of Tribology, ASME* 120: 97–102.
- Ranjith K and Rice JR (1999) Stability of quasi-static slip in a single degree of freedom elastic system with rate and state dependent friction. *Journal of the Mechanics and Physics of Solids* 47(6): 1207–1218.
- Ranjith K and Rice JR (2001) Slip dynamics at an interface between dissimilar materials. *Journal of the Mechanics and Physics of Solids* 49(2): 341–361.
- Renardy M (1992) Ill-posedness at the boundary for elastic solids sliding under Coulomb-friction. *Journal of Elasticity* 27(3): 281–287.
- Rice JR (1983) Constitutive relations for fault slip and earthquake instabilities. *Pure and Applied Geophysics* 121(3): 443–475.
- Rice JR (1999) Flash heating at asperity contacts and rate-dependent friction. *EOS Transactions of the American Geophysical Union* 80: F681.
- Rice JR (2001) New perspectives in crack and fault dynamics. In: Aref H and Phillips JW (eds.) *Mechanics for a New Millennium* (Proceedings of the 20th International Congress of Theoretical and Applied Mechanics, 22 Aug - Sept 2000), pp. 1–23. Chicago: Kluwer.
- Rice JR, Lapusta N, and Ranjith K (2001) Rate and state dependent friction and the stability of sliding between elastically deformable solids. *Journal of the Mechanics and Physics of Solids* 49(9): 1865–1898.
- Rosakis AJ (2002) Intersonic shear cracks and fault ruptures. *Advances in Physics* 51(4): 1189–1257.
- Rosakis AJ, Samudrala O, and Coker D (1999) Cracks faster than the shear wave speed. *Science* 284(5418): 1337–1340.
- Rosakis AJ, Samudrala O, and Coker D (2000) Intersonic shear crack growth along weak planes. *Materials Research Innovations* 3: 236–243.
- Rosakis AJ, Samudrala O, Singh RP, and Shukla A (1998) Intersonic crack propagation in bimaterial systems. *Journal of the Mechanics and Physics of Solids* 46(10): 1789–1813.
- Rubin AM and Gillard D (2000) Aftershock asymmetry/rupture directivity among central San Andreas fault

- microearthquakes. *Journal of Geophysical Research-Solid Earth* 105(B8): 19095–19109.
- Rubin AM and Ampuero J (2006) Aftershock asymmetry on a bimaterial interface. *Journal of Geophysical Research* (to appear).
- Rubinstein S, Cohen G, and Fineberg J (2004) Detachment fronts and the onset of dynamic friction. *Nature* 430: 1005–1009.
- Ruina A (1983) Slip instability and state variable friction laws. *Journal of Geophysical Research* 88(NB12): 359–370.
- Ruppert SD and Yomogida KA (1992) Crack-like rupture model for the 19 September 1985 Michoacan, Mexico, earthquake. *Pure and Applied Geophysics* 138: 407–2.
- Samudrala O, Huang Y, and Rosakis AJ (2002a) Subsonic and intersonic mode II crack propagation with a rate-dependent cohesive zone. *Journal of the Mechanics and Physics of Solids* 50(6): 1231–1268.
- Samudrala O, Huang Y, and Rosakis AJ (2002b) Subsonic and intersonic shear rupture of weak planes with a velocity weakening cohesive zone. *Journal of Geophysical Research-Solid Earth* 107(B8): 10129/2001JB000460.
- Schallamach A (1971) How does rubber slide? *Wear* 17: 301–312.
- Scholz CH (2002) *The Mechanics of Earthquakes and Faulting*, 471 pp. Cambridge: Cambridge University Press.
- Scholz C, Molnar P, and Johnson T (1972) Detailed studies of frictional sliding of granite and implications for earthquake mechanism. *Journal of Geophysical Research* 77(32): 6392–6406.
- Shi ZQ and Ben-Zion Y (2006) Dynamic rupture on a bimaterial interface governed by slip weakening friction. *Geophysical Journal International* 165(2): 469–484.
- Spudich P and Cranswick E (1984) Direct observation of rupture propagation during the 1979 Imperial Valley Earthquake using a short baseline accelerometer array. *Bulletin of the Seismological Society of America* 74(6): 2083–2114.
- Stein RS, Barka AA, and Dieterich JH (1997) Progressive failure on the North Anatolian fault since 1939 by earthquake stress triggering. *Geophysical Journal International* 128(3): 594–604.
- Tullis TE and Goldsby DL (2003) Flash melting of crustal rocks at almost seismic rates. *EOS. Transactions of the American Geophysical Union* 84(46): Fall Meeting Suppl., Abstract S51B-05.
- Thurber, Roecker S, Roberts K, Gold M, Powell L, and Rittger K (2003) Earthquake locations and three-dimensional fault zone structure along the creeping section of the San Andreas fault near Parkfield, CA: Preparing for SAFOD. *Geophysical Research Letters* 30(3): 1112 doi: 10.1029/2002GL016004.
- Uenishi K and Rice JR (2003) Universal nucleation length for slip-weakening rupture instability under nonuniform fault loading. *Journal of Geophysical Research-Solid Earth* 108(B1): 2042 doi: 10.1029/2001JB001681.
- Uenishi K, Rosmanith HP, and Scheidegger AE (1999) Rayleigh pulse-dynamic triggering of fault slip. *Bulletin of the Seismological Society of America* 89(5): 1296–1312.
- Wallace RE (1983) Eyewitness account of surface fault during the earthquake of 28 October 1983 Borah peak, Idaho. *Bulletin of the Seismological Society of America* 74: 1091–1094.
- Weertman J (1980) Unstable slippage across a fault that separates elastic media of different elastic-constants. *Journal of Geophysical Research* 85(NB3): 1455–1461.
- Wu FT, Thomson KC, and Kuenzler H (1972) Stick-slip propagation velocity and seismic source mechanism. *Bulletin of the Seismological Society of America* 62(6): 1621–1628.
- Xia KW, Chalivendra VB, and Rosakis AJ (2006) Observing ideal 'Self-similar' crack growth in experiments. *Engineering Fracture Mechanics* 73: 2748–2755.
- Xia KW, Rosakis AJ, and Kanamori H (2004) Laboratory earthquakes: The sub-Rayleigh-to-supershear rupture transition. *Science* 303 (5665): 1859–1861.
- Xia KW, Rosakis AJ, Kanamori H, and Rice JR (2005) Laboratory earthquakes along inhomogeneous faults: Directionality and supershear. *Science* 308(5722): 681–684.
- Zheng G and Rice JR (1998) Conditions under which velocity-weakening friction allows a self-healing versus a crack-like mode of rupture. *Bulletin of the Seismological Society of America* 88: 1466–1483.
- Zor E, Sandvol E, Gurbuz C, Turkelli N, Seber D, and Barazangi M (2006) The crustal structure of the East Anatolian plateau (Turkey) from receiver functions. *Geophysical Research Letters* 30(24): 8044, doi:10.1029/2003GL018192.